DEPARTMENT OF THE NAVY
DTNSRDC

TWO-DIMENSIONAL SUBSONIC WIND TUNNEL EVALUATION
OF TWO RELATED CAMBERED 15-PERCENT-THICK
CIRCULATION CONTROL AIRFOILS

by

Jane Abramson

APPROVED FOR PUBLIC RELEASE:
DISTRIBUTION UNLIMITED

AVIATION AND SURFACE EFFECTS DEPARTMENT

DTNSRDC ASED-373

September 1977

DAVID
W.
TAYLOR
NAVAL
SHIP
RESEARCH
AND
DEVELOPMENT
CENTER

BETHESDA
MARYLAND
20084

UNCLASSIFIED

SECURITY CLASSIFICATION OF THIS PAGE (When Data Entered)

REPORT DOCUMENTATION PAGE

READ INSTRUCTIONS BEFORE COMPLETING FORM

1. REPORT NUMBER: DTNSRDC/ASED-373
2. GOVT ACCESSION NO.
3. RECIPIENT'S CATALOG NUMBER
4. TITLE (and Subtitle): TWO-DIMENSIONAL SUBSONIC WIND TUNNEL EVALUATION OF TWO RELATED CAMBERED 15-PERCENT THICK CIRCULATION CONTROL AIRFOILS.
5. TYPE OF REPORT & PERIOD COVERED: Final
6. PERFORMING ORG. REPORT NUMBER
7. AUTHOR(s): Jane Abramson
8. CONTRACT OR GRANT NUMBER(s)
9. PERFORMING ORGANIZATION NAME AND ADDRESS: David W. Taylor Naval Ship R&D Center, Aviation & Surface Effects Department, Bethesda, Maryland 20084
10. PROGRAM ELEMENT, PROJECT, TASK AREA & WORK UNIT NUMBERS: Project Element 63203N, Task Area W0578, Work Unit 1619-200
11. CONTROLLING OFFICE NAME AND ADDRESS: Naval Air Systems Command, AIR-320D, Washington, D.C. 20361
12. REPORT DATE: Sep[redacted]977
13. NUMBER OF PAGES: 67
14. MONITORING AGENCY NAME & ADDRESS (if different from Controlling Office)
15. SECURITY CLASS. (of this report): UNCLASSIFIED
15a. DECLASSIFICATION/DOWNGRADING SCHEDULE
16. DISTRIBUTION STATEMENT (of this Report): Approved for Public Release: Distribution Unlimited
17. DISTRIBUTION STATEMENT (of the abstract entered in Block 20, if different from Report)

18. SUPPLEMENTARY NOTES
19. KEY WORDS (Continue on reverse side if necessary and identify by block number): Two-Dimensional Wind Tunnel Testing; Circulation Control Airfoils; Elliptic Airfoil Sections; Tangential Blowing; Boundary Layer Control
20. ABSTRACT (Continue on reverse side if necessary and identify by block number)

Two circulation control cambered elliptic airfoil sections with a thickness-to-chord ratio of 0.15- and 1.0-percent circular arc camber were evaluated subsonically to determine their aerodynamic characteristics. The two models, designated NCCR 1510-7067N and NCCR 1510-7567S, have a common leading edge but different Coanda surfaces. Model NCCR 1510-7067N produced lift coefficients up to 4.65 at $C_\mu = 0.234$; $C_\ell = 4.03$ was attained by

(Continued on reverse side)

DD FORM 1473, 1 JAN 73 EDITION OF 1 NOV 65 IS OBSOLETE
S/N 0102-014-6601

UNCLASSIFIED

SECURITY CLASSIFICATION OF THIS PAGE (When Data Entered)

371 695

(Block 20 continued)

NCCR 1510-7567S at $C_\mu = 0.145$. Model NCCR 1510-7067N was limited in performance by a relatively sharp leading edge that resulted in leading edge separation. Coanda jet-tunnel floor interference, presumably due to effective Coanda turning occurs with model NCCR 1510-7067S at relatively low values of momentum coefficient thereby restricting the test range. Lift-to-equivalent drag ratios in excess of 40 are produced by both configurations at $C_\ell = 1.0$. The ability to produce relatively high lift coefficients essentially independent of angle of attack is indicated by the results of this investigation.

TABLE OF CONTENTS

LIST OF FIGURES

Page

Page

LIST OF TABLES

NOTATION

a_j	Sonic velocity in the jet, ft/sec
C_d	Sectional profile drag coefficient from momentum loss in wake, corrected for additional mass efflux of the jet
$C_{d_{rake}}$	Section profile drag coefficient as measured by rake, uncorrected
C_{d_e}	Equivalent drag coefficient, $C_d + C_\mu(V_j/2V_\infty)$
C_ℓ	Sectional lift coefficient
$C_{\ell_{max}}$	Maximum sectional lift coefficient obtainable within test C_μ limitations
$C_{m_{50}}$	Pitching moment coefficient about the half-chord
C_p	Pressure coefficient, $(P_\ell - P_\infty)/q_\infty$
C_μ	Momentum coefficient, $\dot{m}V_j/(q_\infty S)$
c	Chord length, ft
d	Profile drag corrected for jet mass efflux, lb
d_e	Equivalent drag, lb, $d + \dot{m}V_j^2/(2V_\infty)$
h	Slot height, in
ℓ	Sectional lift, lb
ℓ/d_e	Equivalent section lift-to-drag ratio
M_j	Mach number in the jet
$\dot{m}$	Mass efflux, slug/sec
P_ℓ	Local static pressure on the model, lb/ft^2
P_t	Duct (plenum) total pressure, lb/ft^2
P_∞	Free-stream static pressure, lb/ft^2
q_∞	Free-stream dynamic pressure, lb/ft^2
R	Universal gas constant, 1715 $ft^2/sec^2\ {}^\circ R$
R_e	Reynolds number based on chord

S	Model planform area, ft^2
T_j	Jet static temperature, °R
T_t	Duct (plenum) total temperature, °R
t	Mach thickness, ft
V_j	Jet velocity, ft/sec
V_∞	free stream velocity, ft/sec
x	Chordwise distance from leading edge, ft
x_s	Slot position from leading edge, ft
x/c	Dimensionless chordwise position
α	Geometric angle of attack, deg
γ	Ratio of specific heats

ABSTRACT

Two circulation control cambered elliptic airfoil sections with a thickness-to-chord ratio of 0.15- and 1.0-percent circular arc camber were evaluated subsonically to determine their aerodynamic characteristics. The two models, designated NCCR 1510-7067N and NCCR 1510-7567S, have a common leading edge but different Coanda surfaces. Model NCCR 1510-7067N produced lift coefficients up to 4.65 at $C_\mu = 0.234$; $C_\ell = 4.03$ was attained by NCCR 1510-7567S at $C_\mu = 0.145$. Model NCCR 1510-7067N was limited in performance by a relatively sharp leading edge that resulted in leading edge separation. Coanda jet-tunnel floor interference, presumably due to effective Coanda turning occurs with model NCCR 1510-7067S at relatively low values of momentum coefficient thereby restricting the test range. Lift-to-equivalent drag ratios in excess of 40 are produced by both configurations at $C_\ell = 1.0$. The ability to produce relatively high lift coefficients essentially independent of angle of attack is indicated by the results of this investigation.

ADMINISTRATIVE INFORMATION

The work presented herein was conducted at the David W. Taylor Naval Ship Research and Development Center (DTNSRDC) for the Naval Air Systems Command (AIR 320D) under Project Element 63203N and Task Area W0578.

All data recorded during this experiment were either measured in or converted directly to U.S. customary units. Hence, U.S. customary units are the primary units in this report. Metric units are given adjacent to the U.S. units in parentheses. Angular measurement is the only exception; the unit of degrees is not converted to radians.

INTRODUCTION

Tangential blowing over the bluff trailing edge of two 15-percent cambered elliptic airfoil sections was investigated experimentally. These airfoils are two of a series of five in the circulation control airfoil development program at DTNSRDC[1] that are being used to ascertain the effects of leading and trailing edge geometry on performance. The models have a common leading edge and an interchangeable Coanda surface. All the models employ the Coanda effect to obtain high-lift augmentation by tangentially ejecting a sheet of air near the trailing edge on the upper surface. Because of the Coanda effect, the jet sheet remains attached to the bluff trailing edge and provides a mechanism for boundary layer control. The blowing can be thought of as a movement of the stagnation point thereby producing an increase in circulation.

MODEL AND TEST APPARATUS

The models were constructed with a common leading edge and an interchangeable Coanda surface. Both models are based on an analytically defined ellipse of 15-percent thickness-to-chord ratio and are defined by the following geometric parameters:

	NCCR 1510-7067N	NCCR 1510-7567S
chord	$c = 8.01''$ (20.34 cm)	$c = 7.955''$ (20.3 cm)
circular arc camber	$\delta/c = 0.01$	$\delta/c = 0.01$
slot position	$x_s = 7.75''$ (19.6 cm)	$x_s = 7.75''$ (19.6 cm)
slot/chord ratio	$x_s/c = 0.967$	$x_s/c = 0.974$

A mathematical equation was used to define the rounding of the trailing edge of the pure ellipse for Model NCCR 1510-7067N (see Table 1). The coordinates for this model are listed in Table 2.

---

[1] Wilkerson, J.B., "An Assessment of Circulation Control Airfoil Development," Report DTNSRDC 77-0084 (Aug 1977).

The interchangeable Coanda surface that forms Model NCCR 1510-7067S hereafter referred to as Model 67S, is a spiral. This spiral has its smallest radius of curvature at the slot exit; this is in contrast to Model 67N and other models investigated at DTNSRDC.[2-5] Coordinates for the trailing edge are listed in Table 3.

The outer shell of the model was constructed of wood with an internal steel plenum chamber through which the air for the Coanda jet was introduced. The slot exit is the throat of a converging nozzle formed by the internal geometry of the Coanda surface and the underside of a knife-edged aluminum blade. The slot height was adjusted through the use of pitch screws. An undercut was made in the blade to ensure that the flow would exit tangentially to the model surface (see Figure 1).

The two-dimensional tests were conducted in the 15- x 20-inch subsonic tunnel with a vented test section and plexiglass walls. The models were pressure tapped at center span. Lift and pitching moment coefficients were obtained by numerical integration of pressure tap readings as recorded on a multiple-port scanivalve readout system. These coefficients were corrected by the addition of jet reaction components. Standard solid blockage corrections[6] were applied to the measured free-stream dynamic pressure; no wake blockage factor was used because of the uncertain effects of the jet.

---

[2] Abramson, J., "Two-Dimensional Subsonic Wind Tunnel Evaluation Of A 20-Percent-Thick Circulation Control Airfoil," DTNSRDC Report ASED-331 (Jun 1975).

[3] Williams, R.M. and H.J. Howe, "Two-Dimensional Subsonic Wind Tunnel Tests On A 20-Percent Thick, 5-Percent Cambered Circulation Control Airfoil," NSRDC Report ASED-176 (AD 877-764) (Aug 1970).

[4] Englar, R.J., "Two-Dimensional Subsonic Wind Tunnel Tests Of Two 15-Percent Thick Circulation Control Airfoils," NSRDC Report ASED-211 (Aug 1971).

[5] Englar, R.J., "Two-Dimensional Subsonic Wind Tunnel Tests Of A Cambered 30-Percent Thick Circulation Control Airfoil," NSRDC Report ASED-201 (May 1972).

[6] Pope, A., "Wind-Tunnel Testing," Second Edition, John Wiley and Sons, Inc., New York (1964), pp. 307-311.

Drag measurements were made by using a drag rake placed approximately 1.5 chord lengths downstream of the model inclined at 10 degrees to the free stream. The rake employs 54 total and 8 static tubes, with the heaviest concentration of tubes near the center height. The momentum deficit methods of Betz and Jones[7] were then used to determine the drag coefficient. To account for the additional momentum from the Coanda jet, an addition of $\dot{m}V_\infty/q_\infty S$ was made to the drag coefficient.

To insure that test conditions were as close to two-dimensional flow as possible, especially at high-lift conditions, wall blowing was employed. Two sets of plenums were embedded in each of the tunnel walls: one ahead of the leading edge, the other at approximately the 70-percent chord position. The blowing rates of the two sets of wall jets were adjusted independently and in accordance with the model blowing rate. They were used to energize the wall boundary layer to prevent separation and to reduce the induced effects. Spanwise pressure taps were employed to record the lateral pressure distribution as an indication of the two-dimensionality.

Mass flow rate ($\dot{m}$) was measured by a calibrated orifice plate inserted in the supply line. The jet velocity was calculated by assuming isentropic expansion from duct stagnation pressure to the free-stream static pressure as follows:

$$V_j = a_j M_j = (\gamma R T_j)^{1/2} M_j = \left[2RT_t \left(\frac{\gamma - 1}{\gamma}\right) \left(1 - \left(\frac{P_\infty}{P_t}\right)^{\gamma - 1/\gamma}\right)\right]^{1/2}$$

The momentum coefficient was then defined as $C_\mu = (\dot{m}\, V_j/q_\infty S)$.

A series of runs were made at free-stream dynamic pressures from 10 to 40 psf (478.8 to 1915.2 N/m^2) corresponding to a model Reynolds number range from 0.375×10^6 to 0.52×10^6 for each model (Figures 2 and 3). No significant effect on the data over this Reynolds number range was noted, and q_∞ = 20 psf (957.60 N/m^2) was chosen to allow for a wider range of C_μ, due to limits on the allowable internal duct pressure.

---

[7] Schlichting, Hermann, "Boundary Layer Theory," Sixth Edition, McGraw-Hill Book Company, New York (1968), pp. 708-713.

RESULTS AND DISCUSSION

MODEL NCCR 1510-7067N

The characteristics of a 15-percent cambered ellipse, Model NCCR-7067N, was evaluated for three slot height-to-chord ratios, h/c = 0.0015, 0.0022, and 0.003 (h = 0.012, 0.018, and 0.024 inches, 0.3048, 0.457, and 0.0146 mm) momentum coefficient C_μ ranging from 0 to 0.24, and angles of attack α ranging from -20 to 6 degrees. Figure 4 depicts the variation of momentum coefficient with duct pressure for the three slot height-to-chord ratios and a dynamic pressure of 20 psf (957.60 N/m^2). The expansion of the slot caused by the pressurization of the duct at a slot height-to-chord of 0.0015 is shown in Figure 5. These data were obtained by pressurizing the duct and measuring the resulting slot height with a thickness gage under quiescent tunnel conditions.

Lift

Figures 6 through 8 show the sectional lift coefficient as a function of momentum coefficient for h/c = 0.0015, 0.0022, and 0.003, respectively. For h/c = 0.0015, the coefficient of lift is presented on an expanded scale and as a function of the square root of momentum coefficient in Figures 9 and 10, respectively. In Figure 5, $C_{\ell_{max}}$ = 4.75 is reached at α = -4 degrees at C_μ = 0.227. Examination of the data in this figure indicates an almost identical lift coefficient is obtained at α = -2 and -4 degrees for C_μ >0.10. The experimental data for these two cases indicate an early jet detachment occurred at α = -2 degrees, resulting in some loss in the trailing edge suction peak and possible loss of circulation. For the negative angles of incidence, the lift coefficient continues to increase with increasing C_μ throughout the test range. At positive angles of incidence, however, loss in the leading edge suction peak is noted at some point in the test range, resulting in a "stall" condition. (It should be noted that this condition is localized and is not accompanied by separation on the upper surface.) At zero incidence, a decrease in lift coefficient is observed for C_μ >0.201 and, at first, may be interpreted as indicating a "stall" condition similar to that occurring at α = +2 and +6 degrees. Examination of the pressure plots

(Figure 11) for this case reveals no loss in the leading edge suction peak but does indicate a loss in pressure along the lower surface of the trailing edge. Indications are that this condition is not the result of separation, but rather the influence of the Coanda jet on the lower surface of the model.

Comparisons of lift coefficients for h/c = 0.0015 and 0.0022 for the same value of momentum coefficient and alpha yield interesting results. At $\alpha = 0$ degrees the lift coefficients for the two slot heights are virtually identical until $C_\mu = 0.088$; whereupon a higher C_ℓ is observed for h/c = 0.0022. For the remaining two angles of incidence, at low value of C_μ the lift coefficient obtained at h/c = 0.0015 exceeds that produced at the higher slot height. At $\alpha = -8$ degrees for $C_\mu \gtrsim 0.12$ and at $\alpha = -4$ degrees for $C_\mu \gtrsim 0.16$, a reversal in this trend is noted with a higher C_ℓ being produced at h/c = 0.0022. In comparing the pressure distributions for $\alpha = 0$ and -8 degrees for the two slot height-to-chord ratios, the major difference noted is on the lower surface of the trailing edge. At h/c = 0.0015 a loss in stagnation pressure on the lower trailing edge is apparent in comparison with the larger slot height-to-chord. This again may be attributed to the influence of the Coanda jet. For a slot height-to-chord of 0.003, a significant reduction in lift coefficient for a given value momentum coefficient in relation to both h/c = 0.0015 and 0.0022 is observed.

For $\alpha = -2$, -4, and -8 degrees and h/c = 0.0015, the pressure distributions do not reveal any evidence of leading edge separation bubbles. At $\alpha = -12$ degrees the flow on the lower surface of the leading edge is initially separated and remains so until $C_\mu \approx 0.06$. Initial separation of the entire lower surface occurs at $\alpha = -20$ degrees; no significant attachment begins until $C_\mu = 0.10$.

Figure 12 presents the augmentation ratio as a function of momentum coefficient for h/c = 0.0015. The augmentation ratio is defined as $\Delta C_\ell / C_\mu$, where ΔC_ℓ is the increase in lift coefficient above the unblown value for a given C_μ and incidence. A significant loss of augmentation is apparent at $\alpha = -20$ degrees and $\alpha = +6$ degrees, with the data for the other angles of incidence falling within a relatively narrow band.

The variation of lift coefficient with geometric angle of attack is shown in Figure 13. The slope of the curves are similar for unstalled conditions, and good agreement is seen between the unblown case and the theoretical value predicted for conventional airfoils.

The value of the minimum pressure coefficient on the airfoil as a function of lift coefficient is shown in Figure 14. The minimum pressure coefficient governs the critical Mach number with its attendant high values of drag.

To complete the discussion of the lift characteristics, the effects of spanwise nonuniformity must be considered. Although wall blowing was used to assure spanwise two-dimensionality, the high lift coefficients still produced induced downwash, and therefore a determination of the effective angle of incidence was made. For the experimental cases selected, potential flow pressure distributions for several incidences and an adjusted C_ℓ were produced. The adjustment to the lift coefficient required that the increment of lift due to the jet suction peak be determined and subtracted from the experimental results. Since this increment could not be theoretically predicted, the resulting distributions were then compared to the experimental pressure distribution until leading edge characteristics coincided. The effective angle of incidence for the experimental data is presented in Figure 15.

Drag

The variation of a modified drag coefficient with momentum coefficient for h/c = 0.0015, 0.0022, and 0.003 is presented in Figures 16, 17, and 18. Figure 19 presents the drag variation with momentum coefficient on an expanded scale for h/c = 0.0015. These data result from an integration of the wake deficit using the method of Betz[7] which was then modified to account for the additional momentum of the jet, thereby becoming $C_d = C_{d_{rake}} - (\dot{m} V_\infty / qS)$. The initial unblown drag levels are high due to the nature of bluff trailing edge airfoils. Negative drag levels are achieved at relatively low values of momentum coefficient, with the exception of $\alpha = -20$ degrees. Figure 16 indicates that not only the highest initial value of drag occurs at this incidence, but also an unusually high level of drag persists throughout the entire C_μ range. This is attributed to the extensive flow separation that occurs on the lower surface of the model.

The secondary drag rise, which occurs at $\alpha = +2$ and $+6$ degrees, coincides with the degradation in lift coefficient observed in Figure 6. At $\alpha = 0$ degrees the drag rise coincides with the loss in stagnation pressure on the lower surface of the trailing edge observed in the coefficient of pressure plots, but precedes any degradation in the coefficient of lift. If the loss in stagnation pressure is due to influence of the Coanda jet, then the late detachment would result in mixing losses and a higher drag level. The drag rise observed at $\alpha = 0$ degrees and $h/c = 0.0022$ also coincides with the loss in performance observed in Figure 7.

Pitching Moment

The pitching moment about the midchord ($C_{m_{50}}$) is depicted in Figure 20 as a function of momentum coefficient. The high trailing edge suction peak produces the negative pitching moment, which has been indicative of previous circulation control airfoils.

Equivalent Lift-to-Drag Ratio

The relative performance of a circulation control airfoil section with an unblown airfoil can best be made when the energy expended to produce blowing is accounted for. The equivalent lift-to-drag ratio is presented in Figures 21, 22, and 23 for $h/c = 0.0015$, 0.00226, and 0.003, respectively, as a function of lift coefficient. The equivalent drag is defined as:

$$d_e = d + \frac{P_{comp}}{V_\infty} + \dot{m}\, V_\infty$$

The first term d is the momentum deficit as measured by the drag rake (corrected for jet efflux); the second term is the compressor power and the third term is an intake momentum flux.

The compressor power required may be expressed as:

$$P_{comp} = \frac{\dot{m}}{2} \left(\frac{2\gamma}{\gamma-1}\right) R\, T_d \left[1 - \left(\frac{P_{t_\infty}}{P_t}\right)^{\gamma-1/\gamma}\right]$$

For subsonic flows with $M_\infty \leq 0.2$, $P_{t_\infty} = P_\infty$ and the above becomes:

$$P_{comp} = \frac{1}{2}\, \dot{m}\, V_j^2$$

Substituting for P_{comp}, the coefficient form becomes:

$$\frac{\ell}{d_e} = \frac{C_\ell}{C_d + C_\mu \dfrac{V_j}{2V_\infty} + C_\mu \dfrac{V_\infty}{V_j}}$$

The maximum ℓ/d_e generated was approximately 45 at $C_\ell = 0.75$, despite the relatively high value of maximum lift coefficients. Maximum efficiency is generated at positive angles of incidence and low blowing. It is also f. und that the maximum ℓ/d_e for negative angles of incidence occurs at low values of momentum coefficient. These results emphasize the need to produce high values of lift coefficient at low values of momentum coefficient in order to maintain high efficiency due to the prominence of the kinetic energy term ($C_\mu V_j/2V_\infty$).

When comparing the results for the various slot heights, it should be noted that the ℓ/d_e is lowest at h/c = 0.0030. The efficiency of the model at h/c = 0.0022 is slightly greater than at h/c = 0.0015.

MODEL NCCR 1510-7567S

Lift

The characteristics of the spiral trailing edge configuration (designated NCCR 1510-7567S) were investigated experimentally for three slot height-to-chord ratios of 0.0012, 0.0015, and 0.00226 (h = 0.008, 0.012, and 0.018 inch; 0.203, 0.3048, 0.457 mm) over an angle-of-attack range -20 degrees $\leq \alpha \leq$ +10 degrees for $0 \leq C_\mu \leq 0.18$. The range of momentum coefficients was limited because of the early impingement of the jet on the tunnel floor, presumably due to effective Coanda turning. The expansion of the slot height caused by the pressurization of the duct for h/c = 0.0015 is presented in Figure 24. Figure 25 indicates the variation of momentum coefficient with duct pressure for the three slot height-to-chord ratios.

Figures 26, 27, and 28 present the sectional lift coefficients as a function of momentum coefficient for the three slot height-to-chord ratios. For h/c = 0.0015 the lift coefficient is presented on an expanded scale and as a function of the square root of momentum coefficient in Figures 29 and 30, respectively. Although all data recorded are included for completeness, a hatch mark appears in those figures to indicate the point at which disturbance of a set of floor tufts placed behind the model was visually noted. Since verification was visual, there is the possibility of interference effects occurring before the hatch mark.

As indicated in Figure 26, at α = +10, +6, and +2 degrees, $C_{\ell_{max}}$ occurs at progressively lower values of momentum coefficient followed by a "C_μ stall". At α = +10 degrees the pressure plots indicate the existence of a leading edge separation bubble until a blowing level of C_μ = 0.03 is reached.

A comparison of the results obtained in Figures 27 and 28 for h/c = 0.001 and 0.00226 indicates a degradation of performance in relation to those obtained at h/c = 0.0015. At h/c = 0.001 the plots of pressure coefficient on the airfoil indicate a lower value of the trailing edge suction peak; and at the higher values of C_μ, there is a noticeably lower level of suction on the upper surface, as compared to h/c = 0.0015. To a more limited extent, the same behavior is observed when comparing the results obtained at h/c = 0.0022 with those at h/c = 0.0015. At some point in the test range, the differences observed between the two slot heights diminish, and the results at higher values of C_μ become approximately the same.

In an attempt to extend the range of momentum coefficient, the model with h/c = 0.0015 was raised 1.6 inches (40.64 mm) towards the tunnel ceiling. Although this resulted in some interference on the model upper surface, it also eliminated the "stall like" characteristics for a limited increase in C_μ, as seen in Figure 31. The $C_{\ell_{max}}$ increased from 3.85 to 4.24 at $\alpha = 0$ degrees and from 4.03 to 4.53 at $\alpha = -2$ degrees.

Figure 32 depicts the augmentation ratio for h/c = 0.0015 as a function of momentum coefficient. A significant loss of augmentation is seen at $\alpha = -20$ degrees and at $\alpha = +10$ degrees. As with the previous configuration, an examination of the pressure distribution at $\alpha = -20$ degrees indicates that initially the flow along the entire lower surface is separated and complete attachment does not occur until $C_\mu = 0.12$. The loss in augmentation at $\alpha = +10$ degrees coincides with the degradation of performance already noted in Figure 26.

The variation of the lift coefficient with angle of attack is presented in Figure 33. At the lower values of momentum coefficient, the results are very similar to those obtained with the previous configuration. The first noticeable difference occurs at $C_\mu = 0.050$ and $\alpha = +2$ and +6 degrees where the coefficient of lift for Model 67S is lower than that produced by Model 67N. This pattern persists at $C_\mu = 0.10$, although a higher C_ℓ is produced by Model 67S at $\alpha = -2$ and 0 degrees. This could be attributed to the effects of jet-tunnel floor interference, the onset of which is alpha dependent to a limited extent. The effective angle of incidence for this configuration was determined as previously discussed, and the results are presented in Figure 34.

Figure 35 presents the value of the minimum pressure coefficient as a function of lift. Comparing these results to those obtained for the previous configuration, it should be noted that a higher C_ℓ can be obtained for the same value of $C_{P_{min}}$.

Drag

Figure 36 presents the variation of the modified coefficient of drag with momentum coefficient for h/c = 0.0015. An expanded scale plot for low values of C_μ is presented in Figure 37. As was previously the case, the unblown drag levels are high; however, except for $\alpha = +10$ degrees, an immediate reduction is noted for all angles of incidence. In this case a leading edge separation bubble followed by "C_μ stall" would tend to prevent drag reduction. The data to the right of the hatch mark again represent data points where jet-tunnel floor interference is known to occur. A drag rise is noted beyond this point at all angles of attack. A comparison of these results to those presented in Figure 15 shows a lower drag level is achieved by Model 67N at all angles of incidence except α = +6 degrees for $C_\mu \geq .06$. This can be attributed to the more effective Coanda turning (which was probably achieved by Model 67S) that produced greater mixing losses with the free stream and jet-tunnel floor interference.

The variation of drag with momentum coefficient for h/c = 0.001 and 0.00226 is depicted in Figure 38 and 39.

Pitching Moment

Pitching moment coefficient as a function of momentum coefficient is presented in Figure 40. The spiral trailing edge produced a lower jet suction peak for a given C_ℓ or C_μ than the previous configuration, which resulted in a less negative pitching moment. This trend was not expected due to the high radius of curvature at the slot exit which is characteristic of this design. The reflex in the moment curves observed at the higher values of momentum coefficients and negative angles of incidence is the result of the influence of the jet on the lower surface of the trailing edge which produces a loss of stagnation pressure.

Equivalent Lift-to-Drag Ratio

The equivalent lift-to-drag ratio as a function of C_ℓ is presented in Figures 41, 42 and 43 for h/c = 0.0015, 0.001, and 0.00226, respectively. In general, both configurations resulted in very similar curves with the maximum efficiency achieved at positive angle of incidence. A loss in efficiency is noted in data taken after the onset of jet-tunnel floor interference due mainly to a large increase in the measured drag level.

A comparison of ℓ/d_e for h/c = 0.00226 and 0.0015 indicates a higher maximum efficiency is obtained at the smaller slot height for α = 0 and -4 degrees while the maximum ℓ/d_e at α = -8 degrees is approximately the same. The lowest efficiency for this configuration is obtained at h/c = 0.001.

CONCLUSIONS

An attempt was made to experimentally ascertain the effect of trailing edge geometry on two, otherwise identical, 15-percent cambered ellipses. Due to the early onset of interference between the jet and the tunnel floor for Model NCCR 1510-7567S, the test range was limited. This, in turn, limited the obtainable value of $C_{\ell_{max}}$, while producing relatively high values of C_d.

For both configurations at the lower values of momentum coefficients, C_ℓ, C_d, and ℓ/d_e are very similar. The difference between the configurations noted thus far concerns the pitching moment and minimum pressure coefficient. Model NCCR 1510-7567S, with its lower trailing edge suction peak, has a less negative pitching moment and a more positive value of $C_{p_{min}}$ for a given value of C_ℓ than does Model NCCR 1510-7067N. The pitching moment is important from the standpoint of controllability, while $C_{p_{min}}$ governs the critical Mach number.

The following conclusions can be drawn from the experimental data

- For the spiral trailing edge configuration (Model NCCR 1510-7567S), a $C_{\ell_{max}}$ = 4.03 was generated at C_μ = 0.145. The experiment indicates that higher values of $C_{\ell_{max}}$ can be generated if sufficient clearance between the model and the tunnel floor could be provided. Augmentation ratios in excess of 50, as well as maximum efficiencies in excess of 40, were produced. Drag levels were higher at $C_\mu \geq 0.06$ than those produced by Model 67N; however, this may be due to jet-tunnel floor interference.
- Model NCCR 1510-7067N generated maximum lift coefficients up to 4.65 at C_μ = 0.234. A maximum lift augmentation of approximately 60 was also produced. The initially high drag coefficients were reduced at relatively low levels of momentum coefficients.

- The effect of slot height on performance is varied. Neither increasing or decreasing the slot height-to-chord ratio increases the sectional lift coefficient over that obtained at h/c = 0.0015 for Model NCCR 1510-7567S. For Model NCCR 1510-7067N increasing the slot height-to-chord ratio from 0.00149 to 0.00224 results in an increase in $C_{\ell_{max}}$. This is due mainly to a loss in stagnation pressure on the lower surface of the trailing edge at the smaller slot height-to-chord ratios.

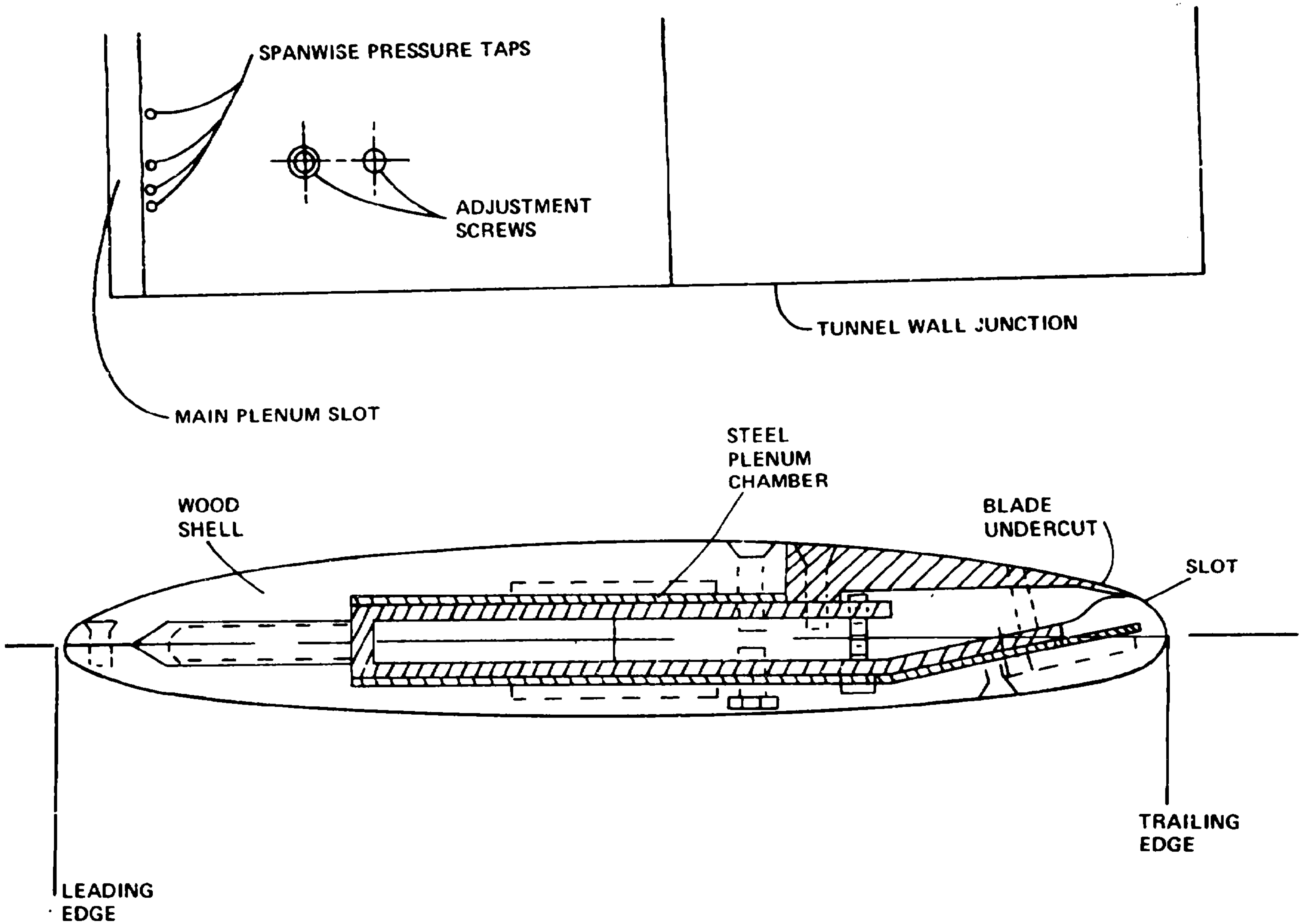

Figure 1 - Two-Dimensional Model Geometry

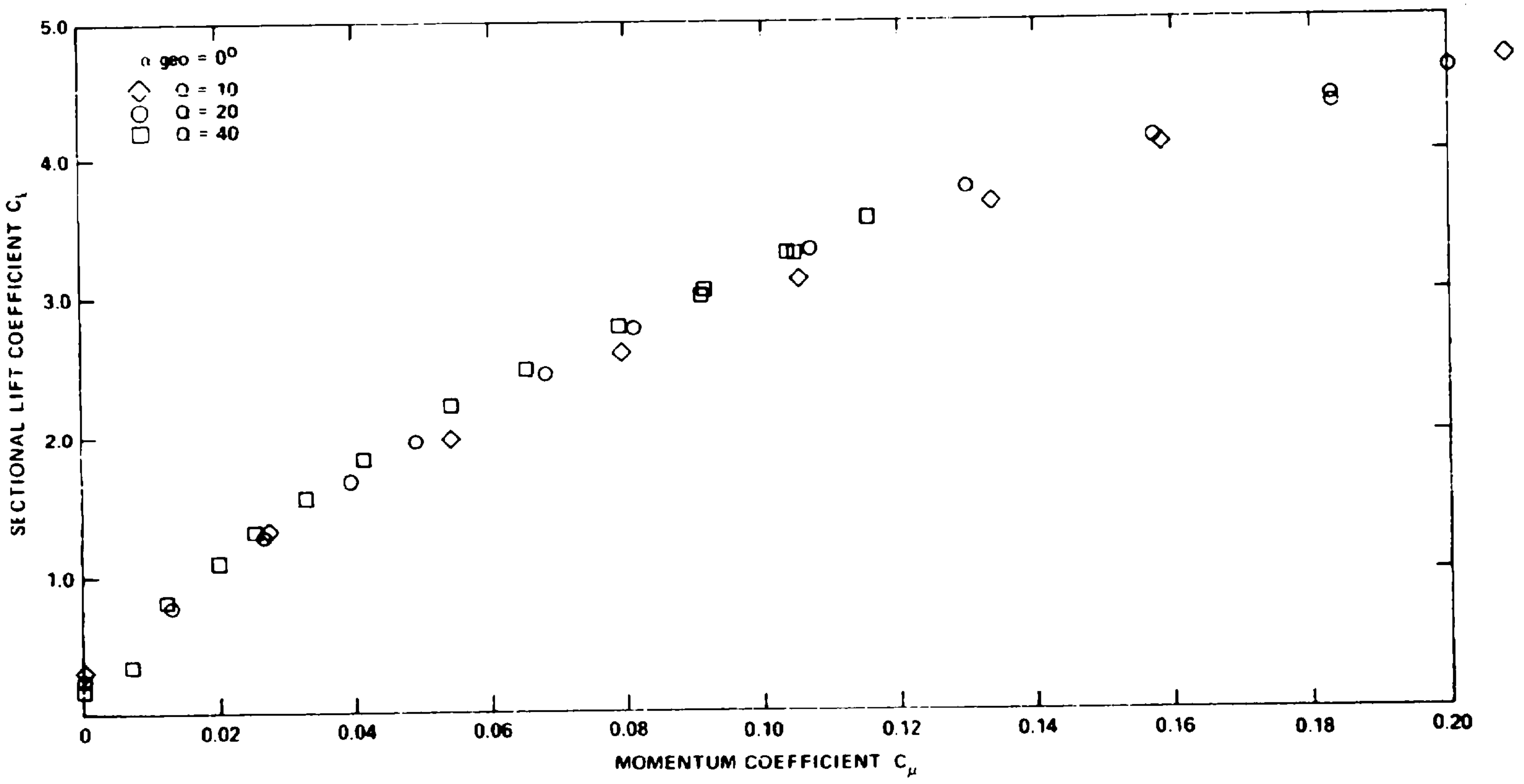

Figure 2 - Model NCCR 1510-7067N Lift Variation with Dynamic Pressure

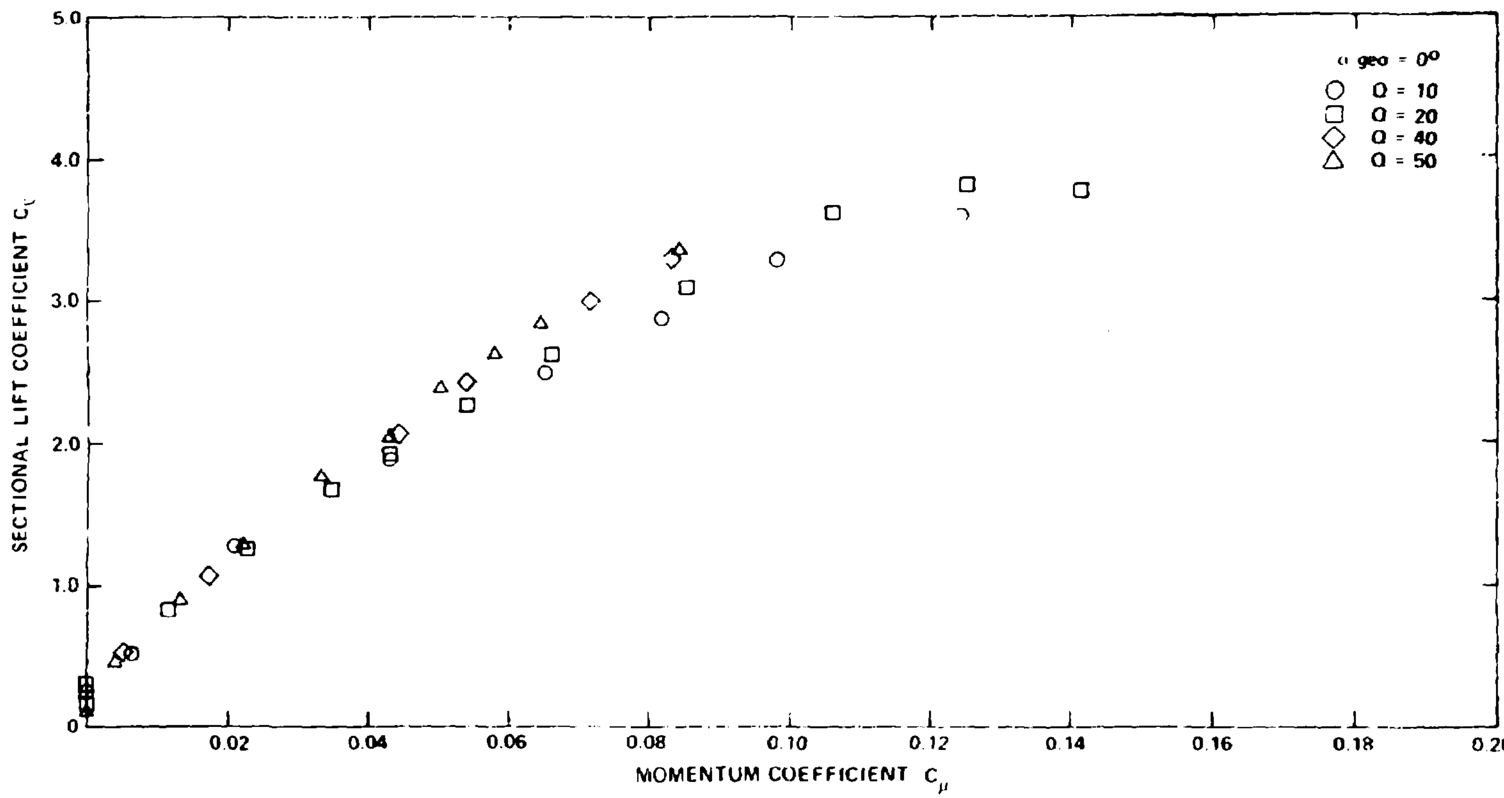

Figure 3 - Model NCCR 1510-7567S Lift Variation with Dynamic Pressure

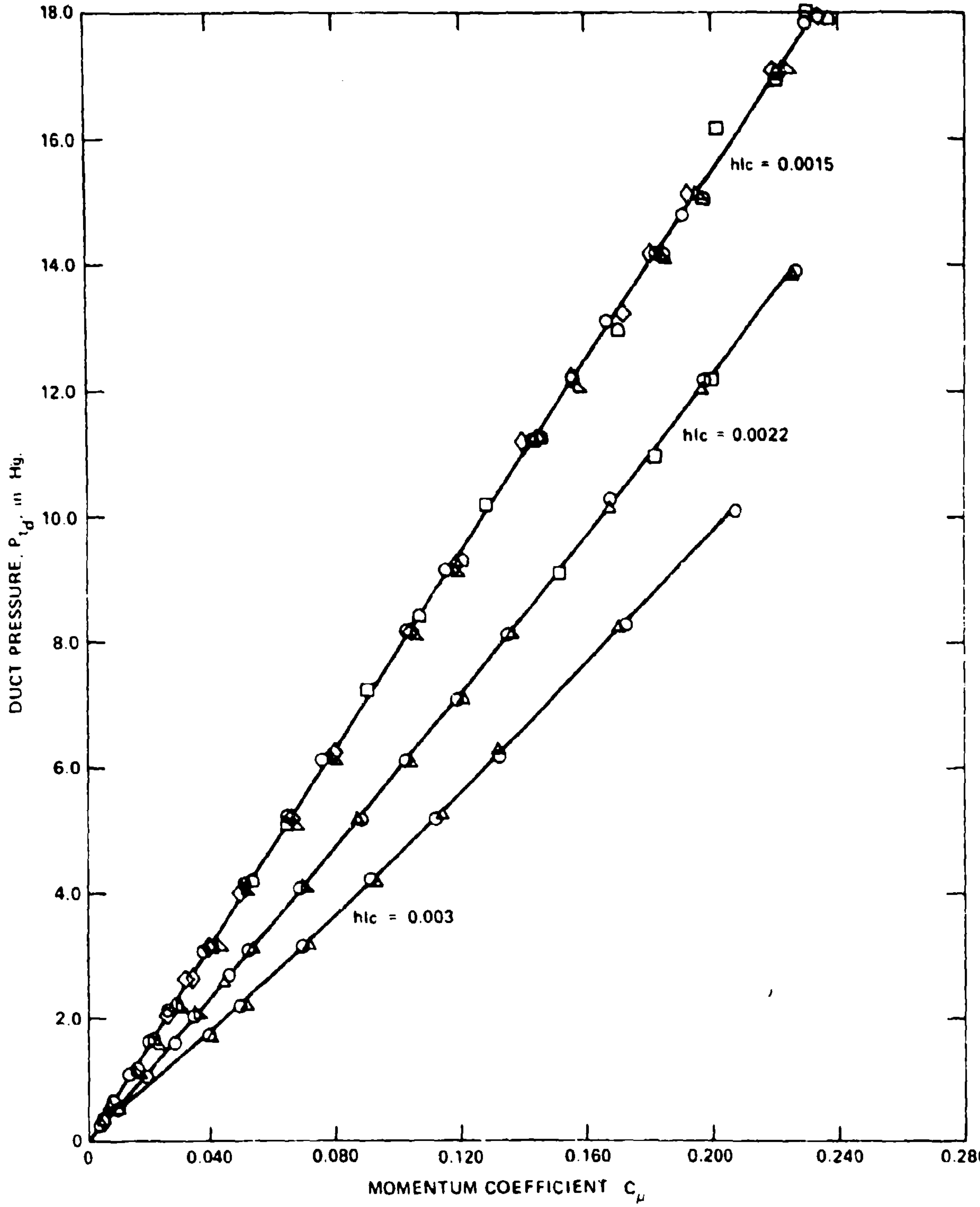

Figure 4 - Variation of Momentum Coefficient with Duct Pressure and Slot Height

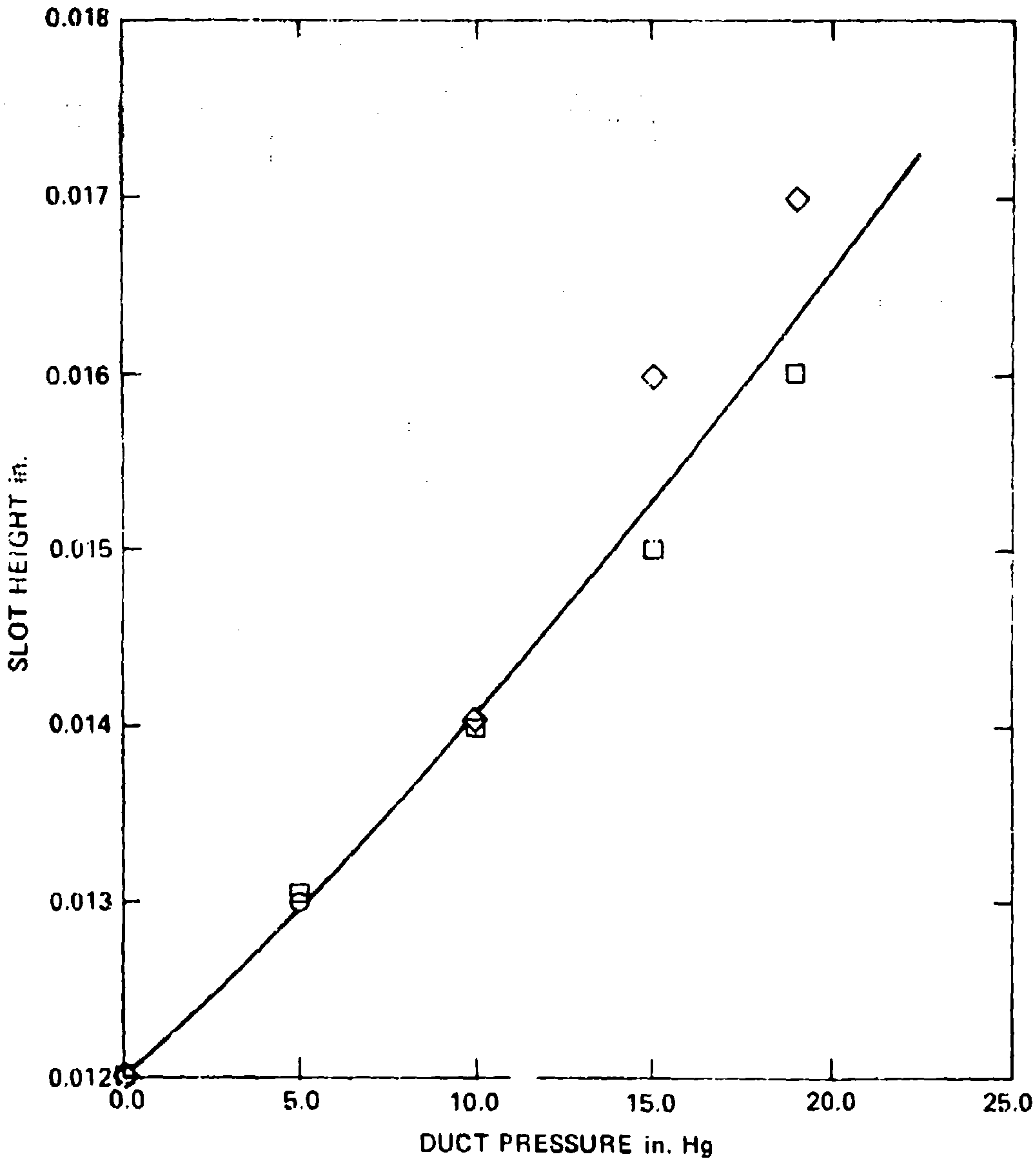

Figure 5 - Variation of Slot Height with Duct Pressure

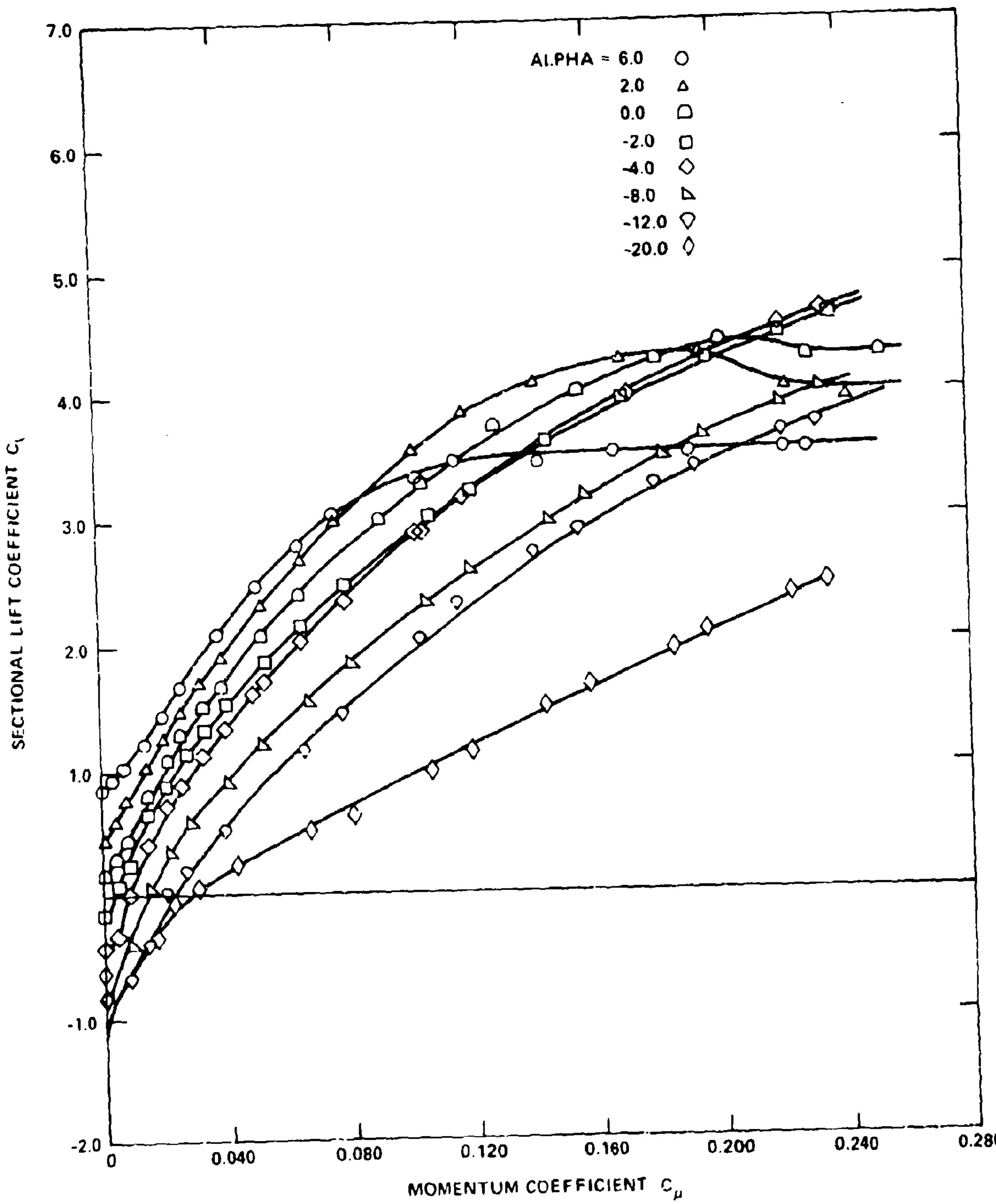

Figure 6 - Model NCCR 1510-7067N Lift Variation with Momentum Coefficient, h/c = 0.0015

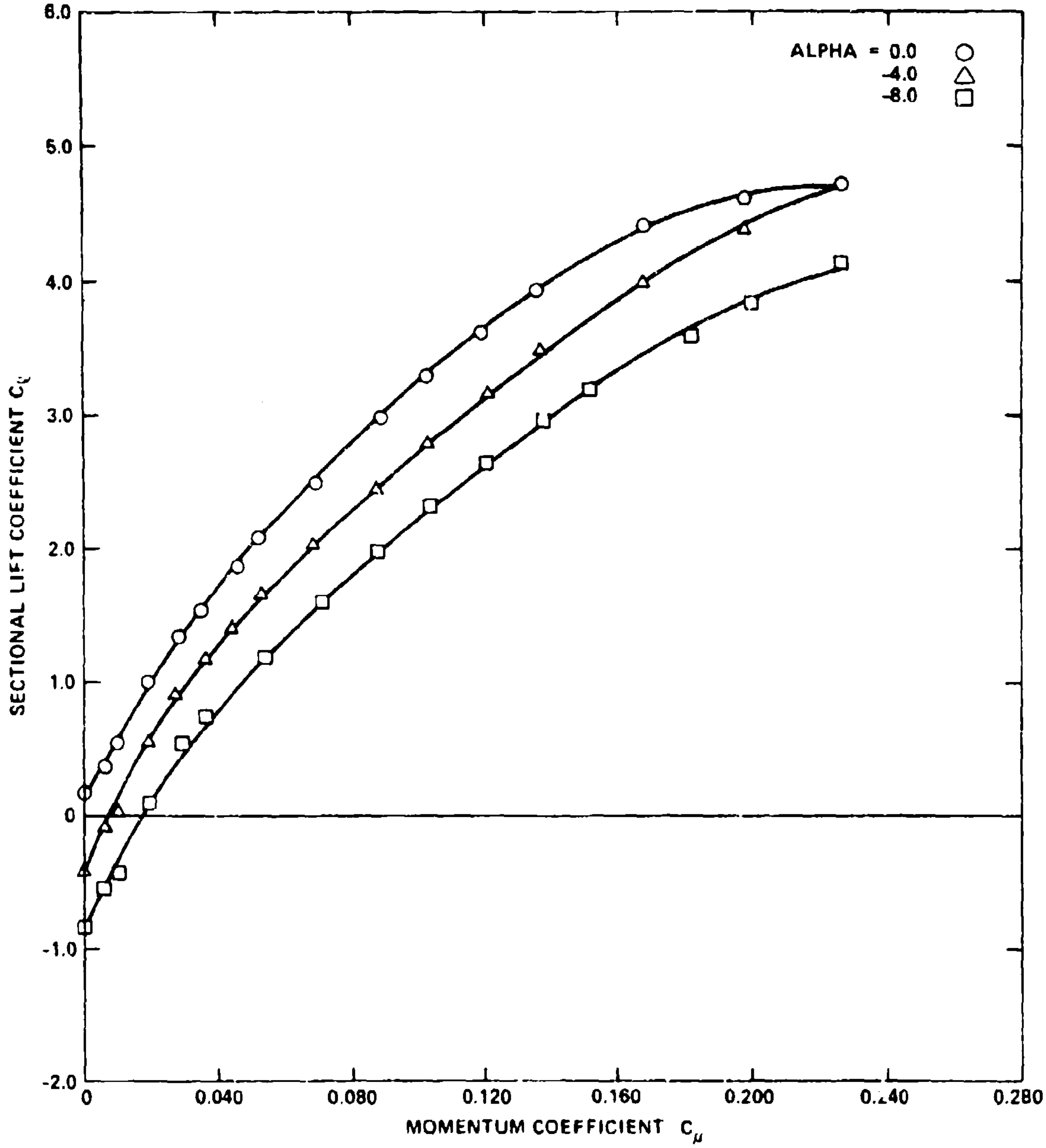

Figure 7 - Model NCCR 1510-7067N Lift Variation with Momentum Coefficient, h/c = 0.0022

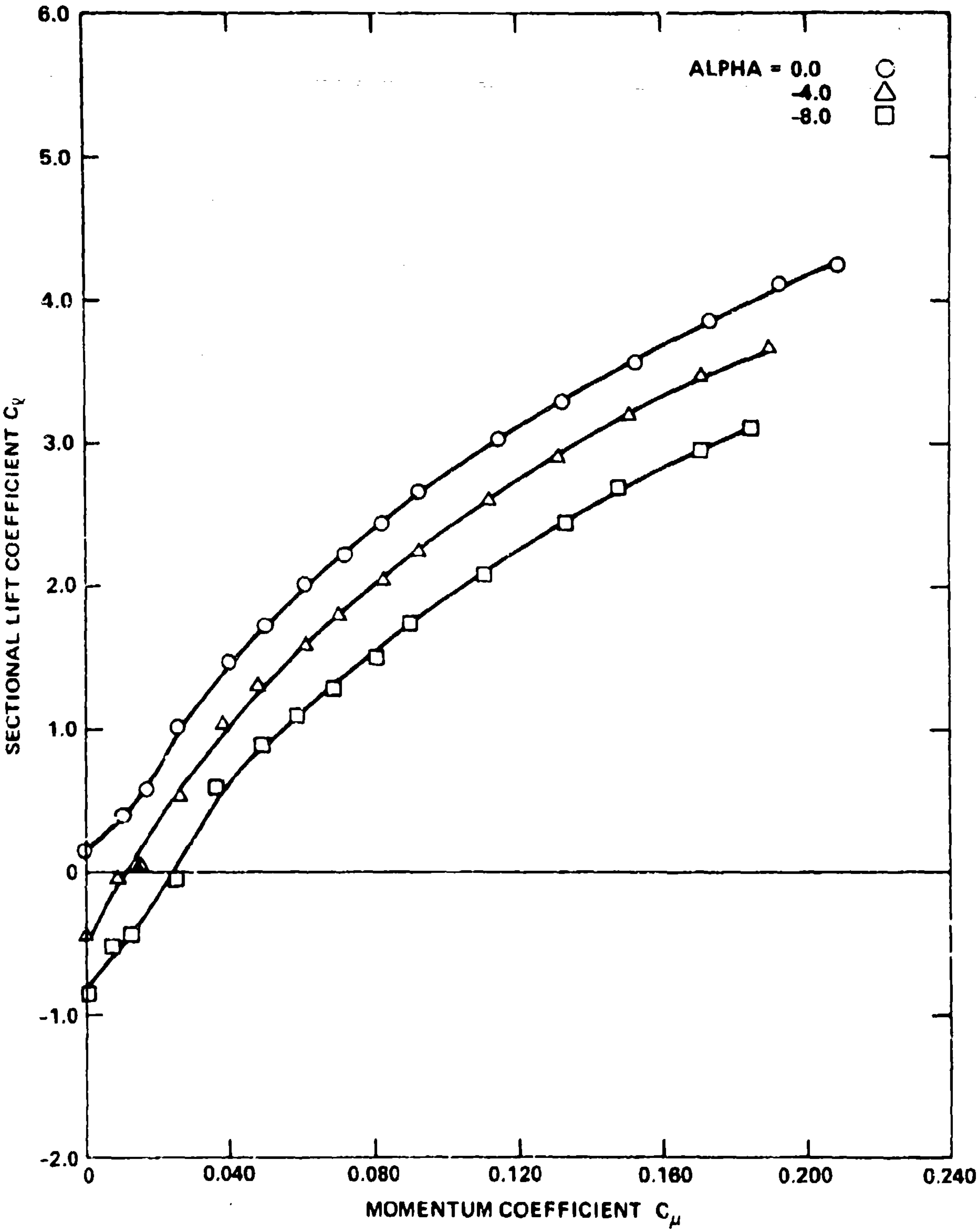

Figure 8 - Model NCCR 1510-7067N Lift Variation with Momentum Coefficient, h/c = 0.003

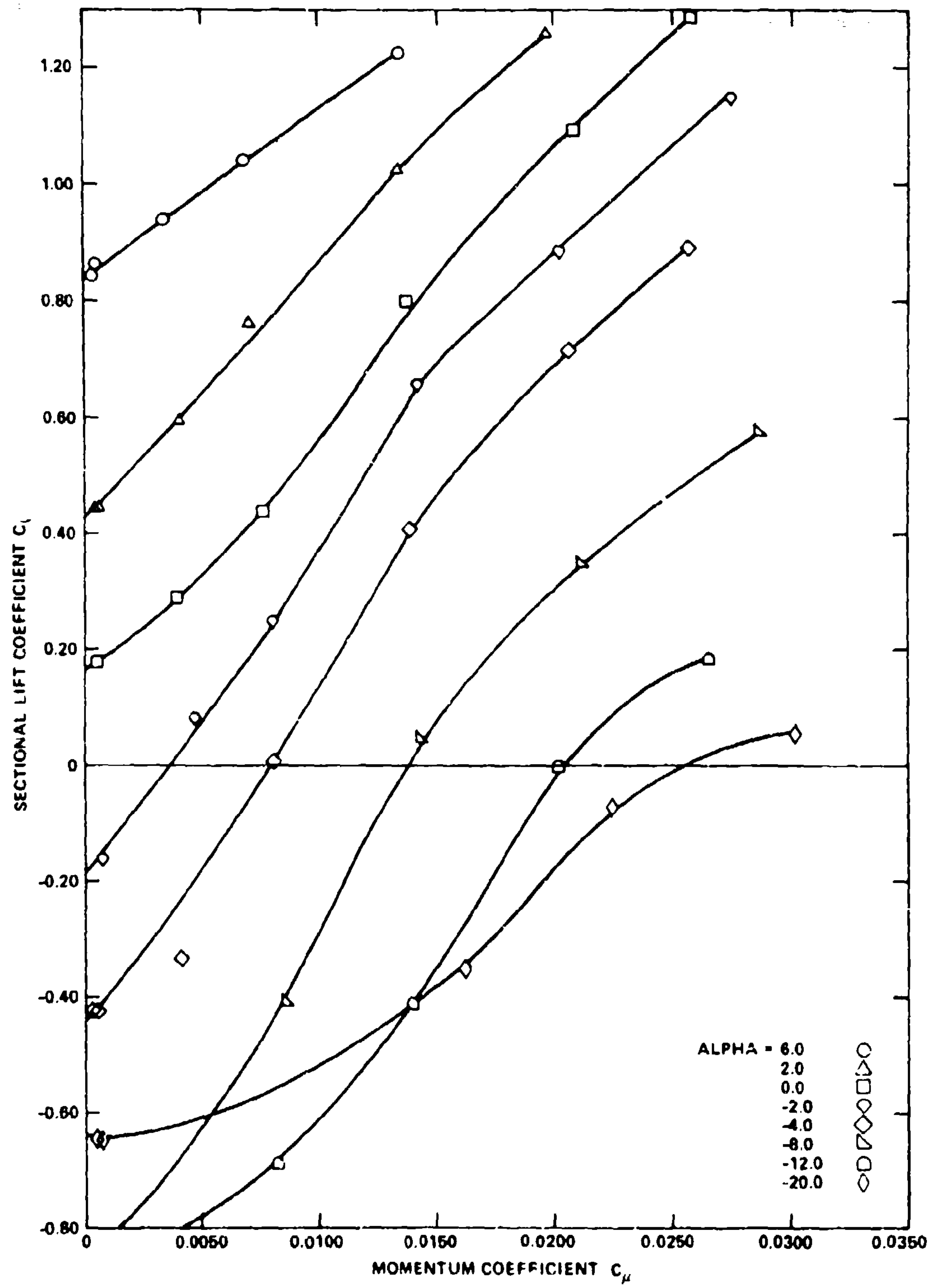

Figure 9 - Model NCCR 1510-7067N Lift Variation with Momentum Coefficient, h/c = 0.0015 (Expanded Scale)

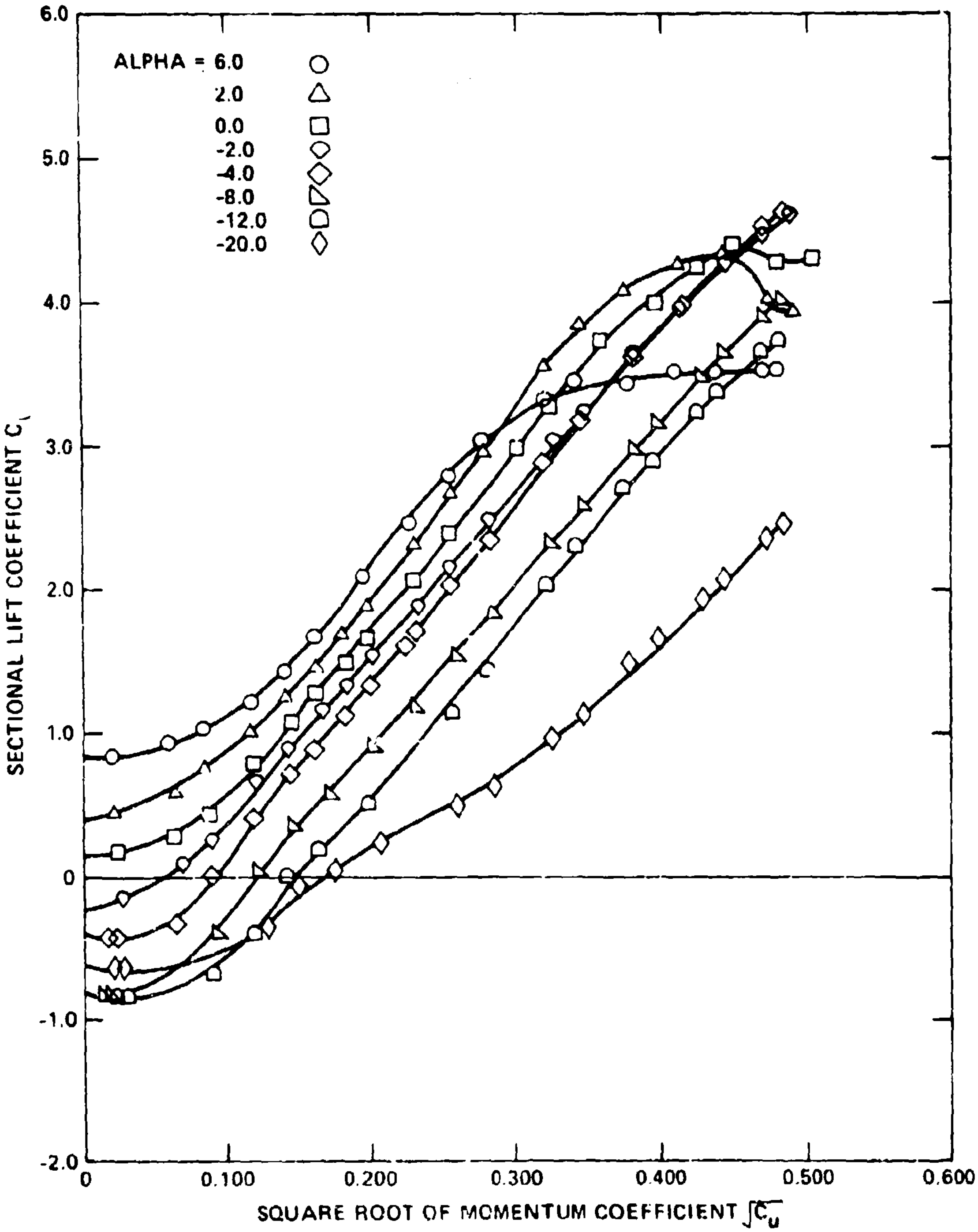

Figure 10 - Model NCCR 1510-7067N Lift Variation with the Square Root of Momentum Coefficient, h/c = 0.0015

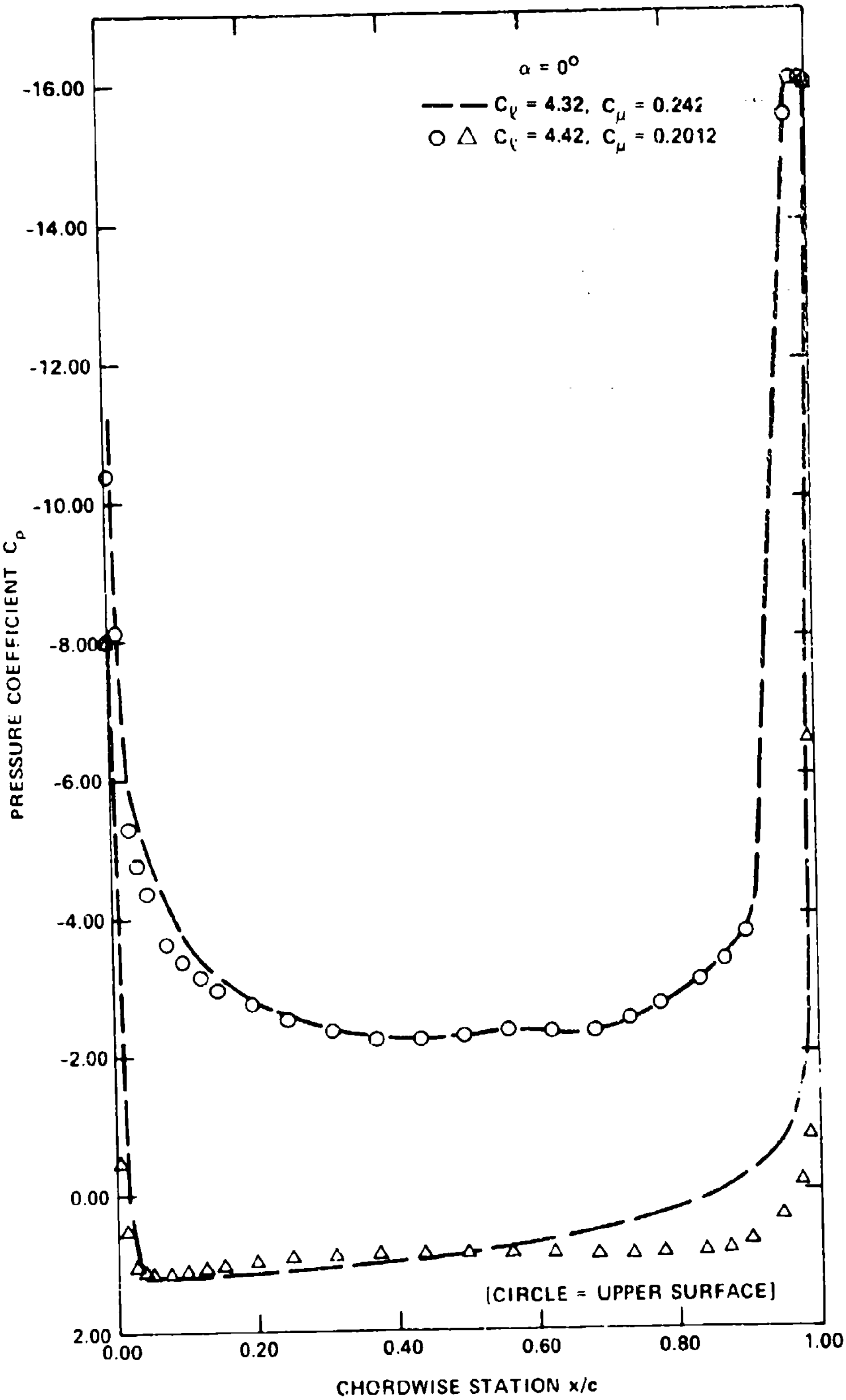

Figure 11 - Model NCCR 1510-7067N Experimental Pressure Distribution at Zero Geometric Incidence (α = 0°)

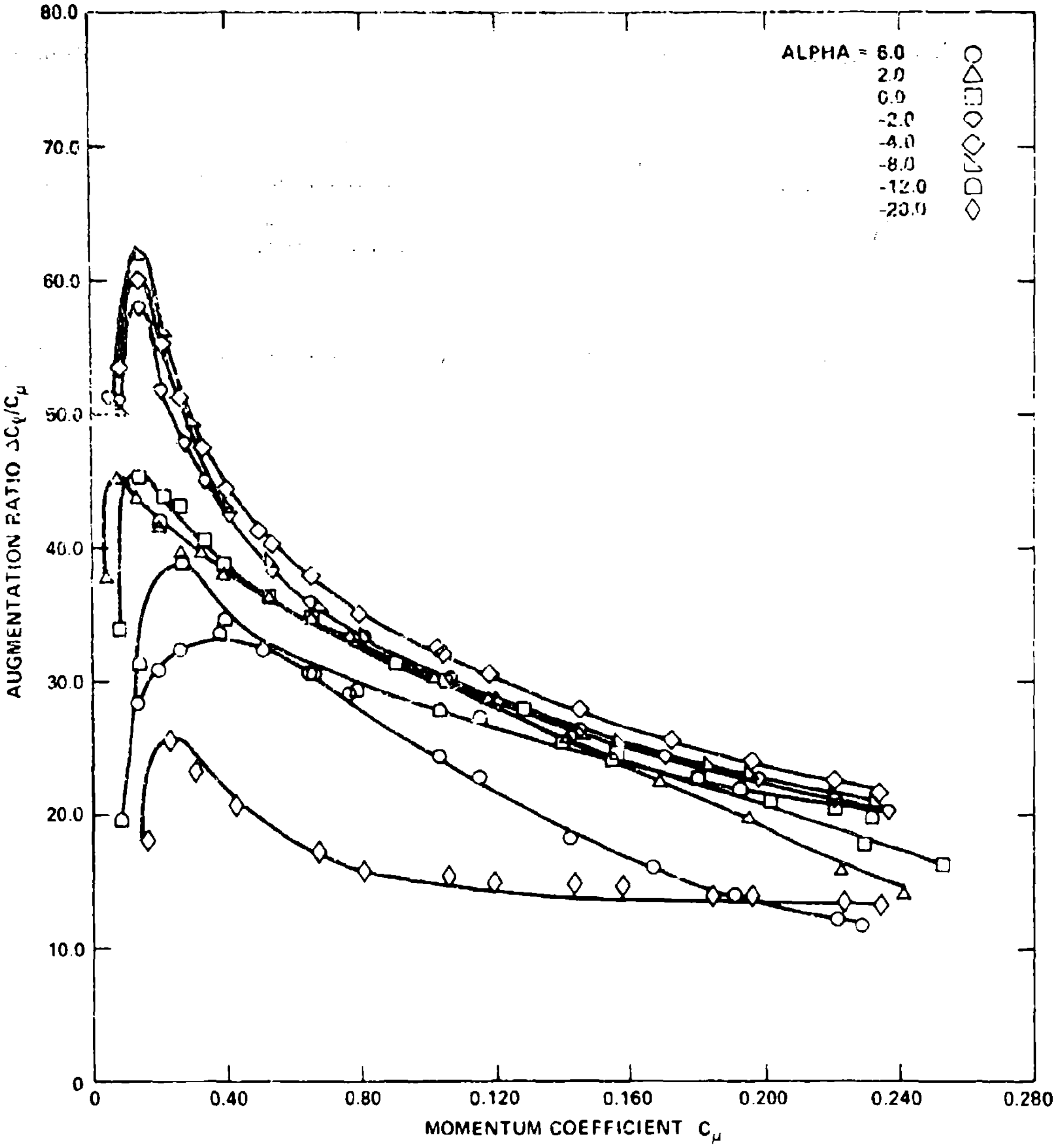

Figure 12 - Model NCCR 1510-7067N Lift Augmentation, $h/c = 0.0015$

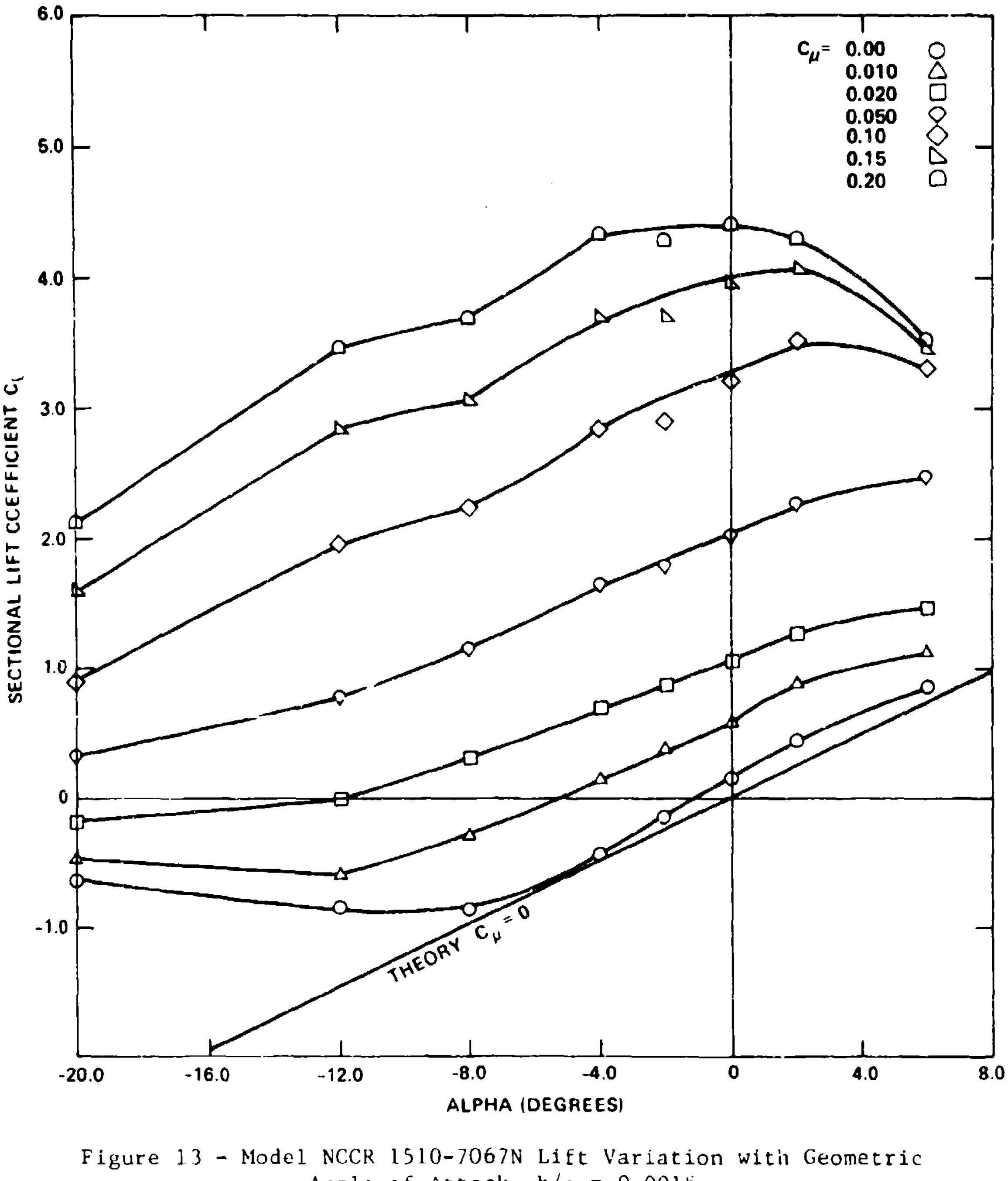

Figure 13 - Model NCCR 1510-7067N Lift Variation with Geometric Angle of Attack, h/c = 0.0015

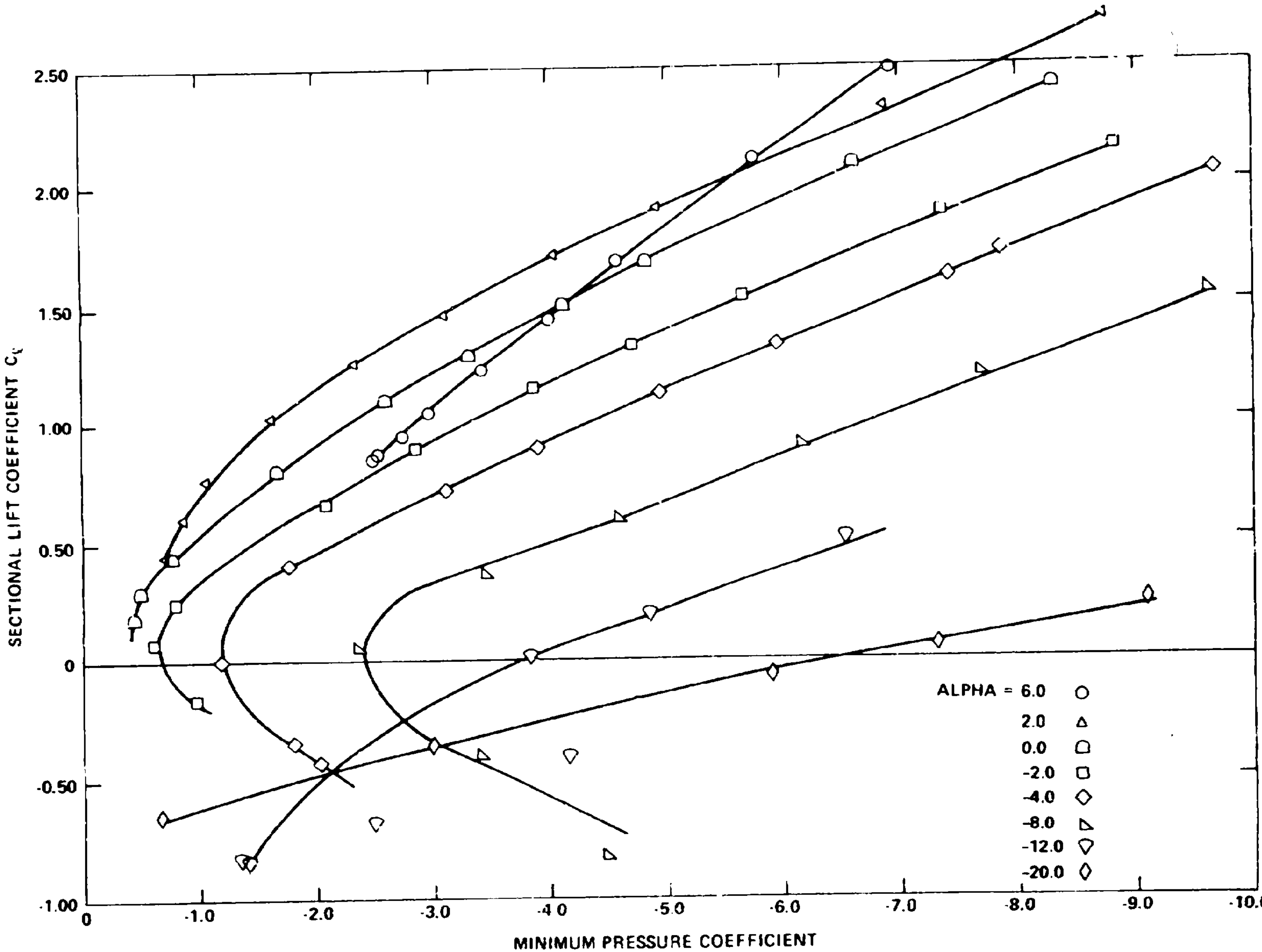

Figure 14 - Model NCCR 1510-7067N Minimum Pressure Coefficient, h/c = 0.0015

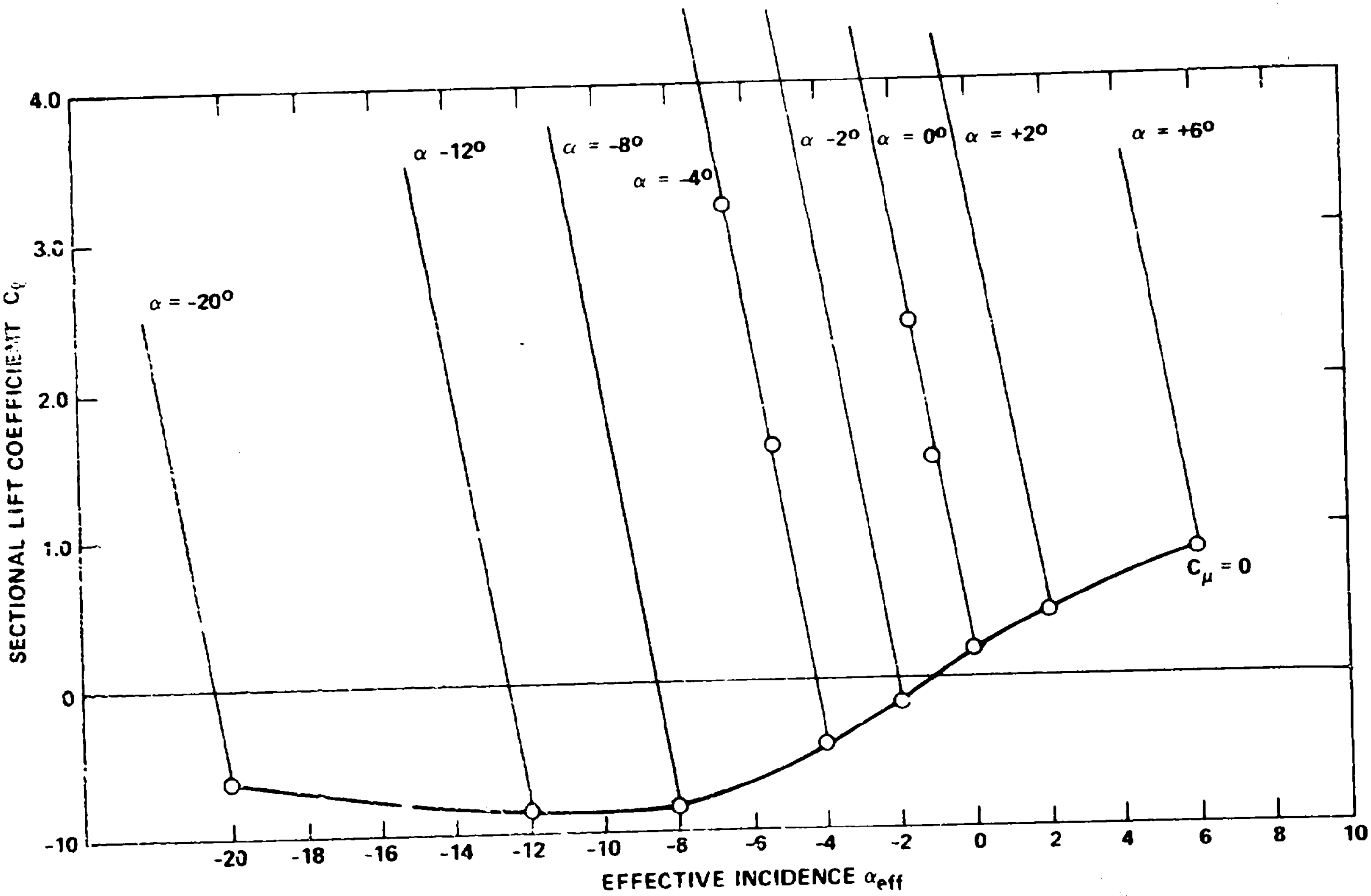

Figure 15 - Model NCCR 1510-7067N Induced Angle Corrections to Geometric Incidence

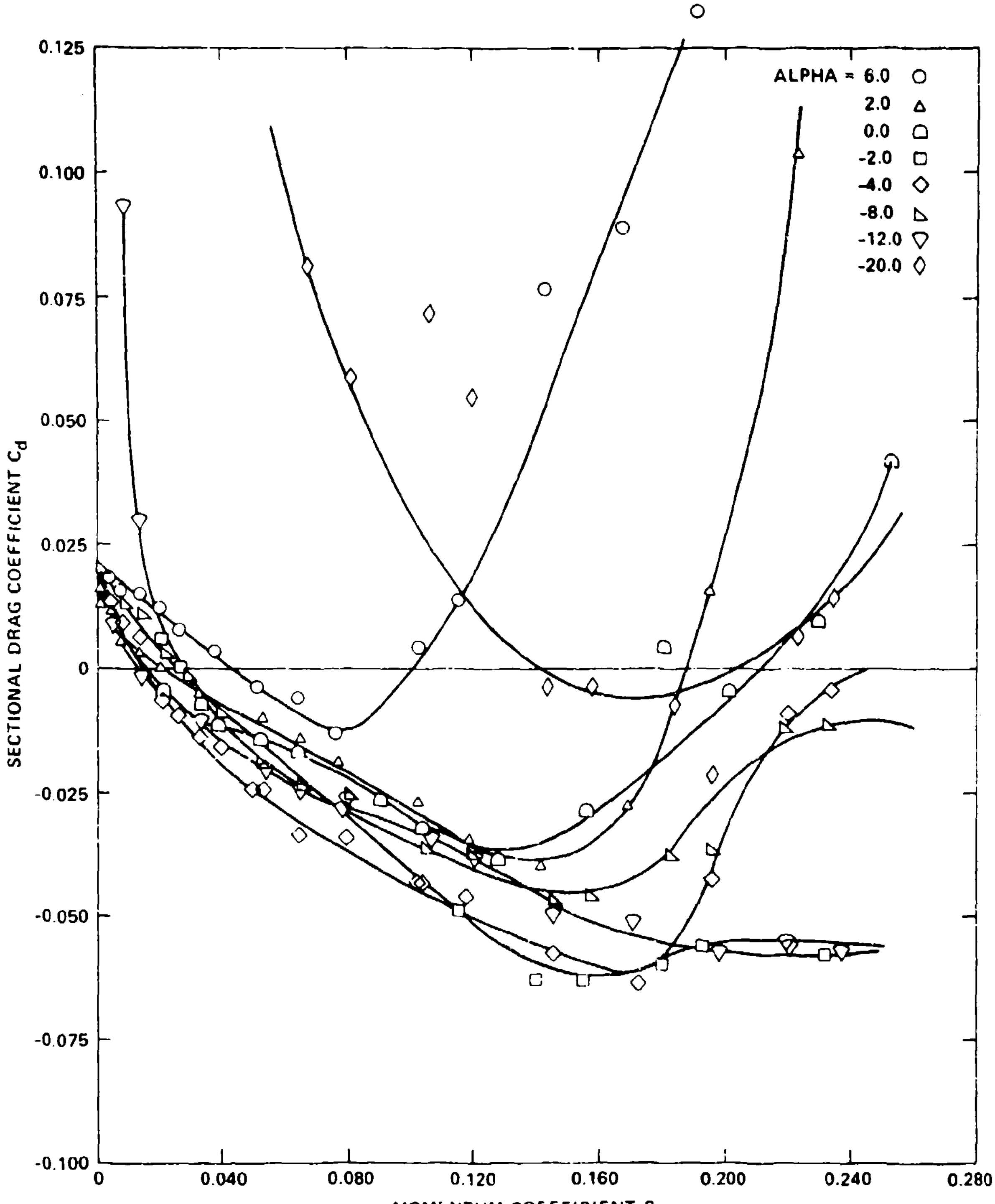

Figure 16 - Model NCCR 1510-7067N Drag Coefficient Variation with Momentum Coefficient, h/c = 0.0015

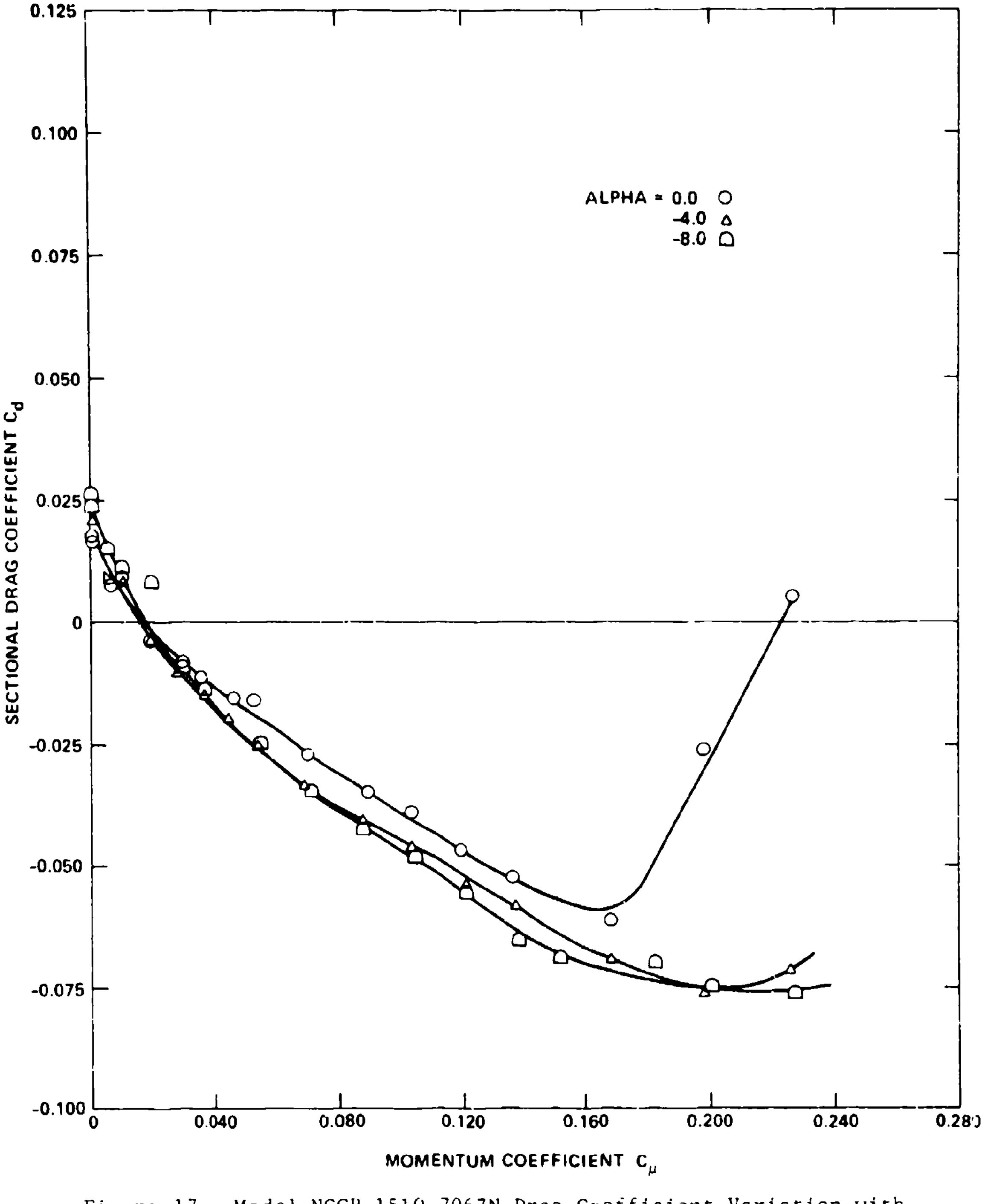

Figure 17 - Model NCCR 1510-7067N Drag Coefficient Variation with Momentum Coefficient, h/c = 0.0022

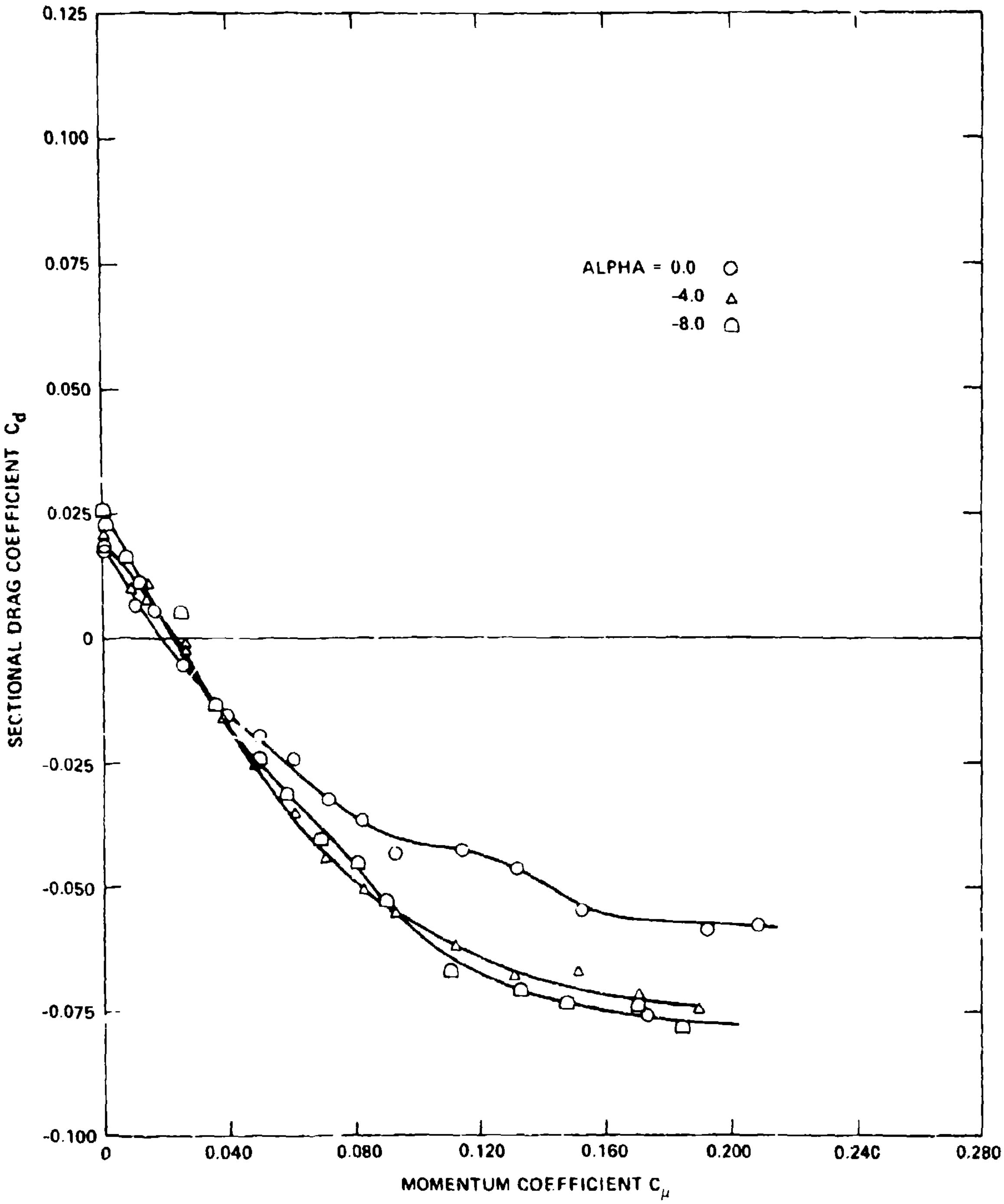

Figure 18 - Model NCCR 1510-7067N Drag Coefficient Variation with Momentum Coefficient, h/c = 0.003

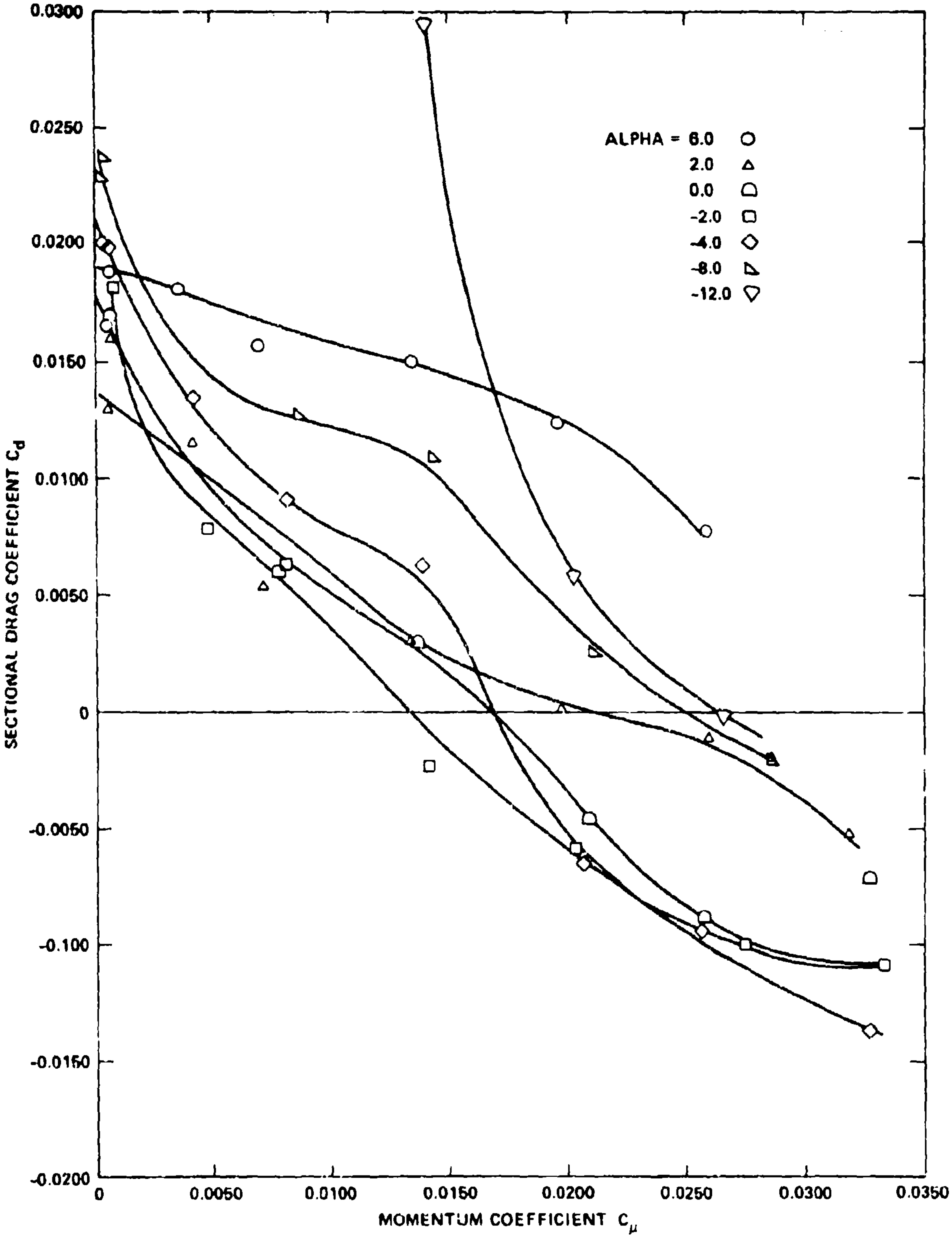

Figure 19 - Model NCCR 1510-7067N Drag Coefficient Variation with Momentum Coefficient, h/c = 0.0015 (Expanded Scale)

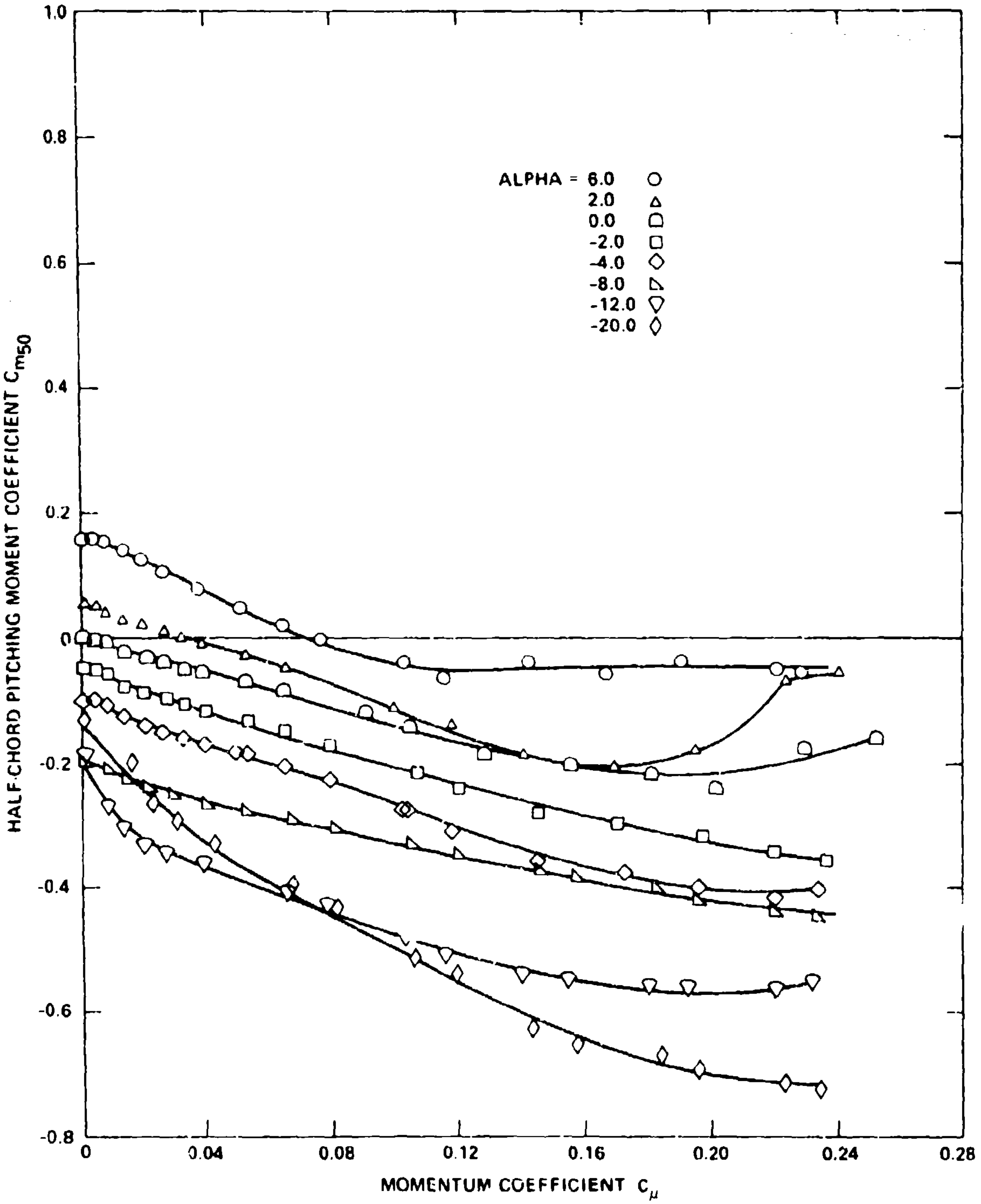

Figure 20 - Model NCCR 1510-7067N Variation in Half-Chord Pitching Moment Coefficient, h/c = 0.0015

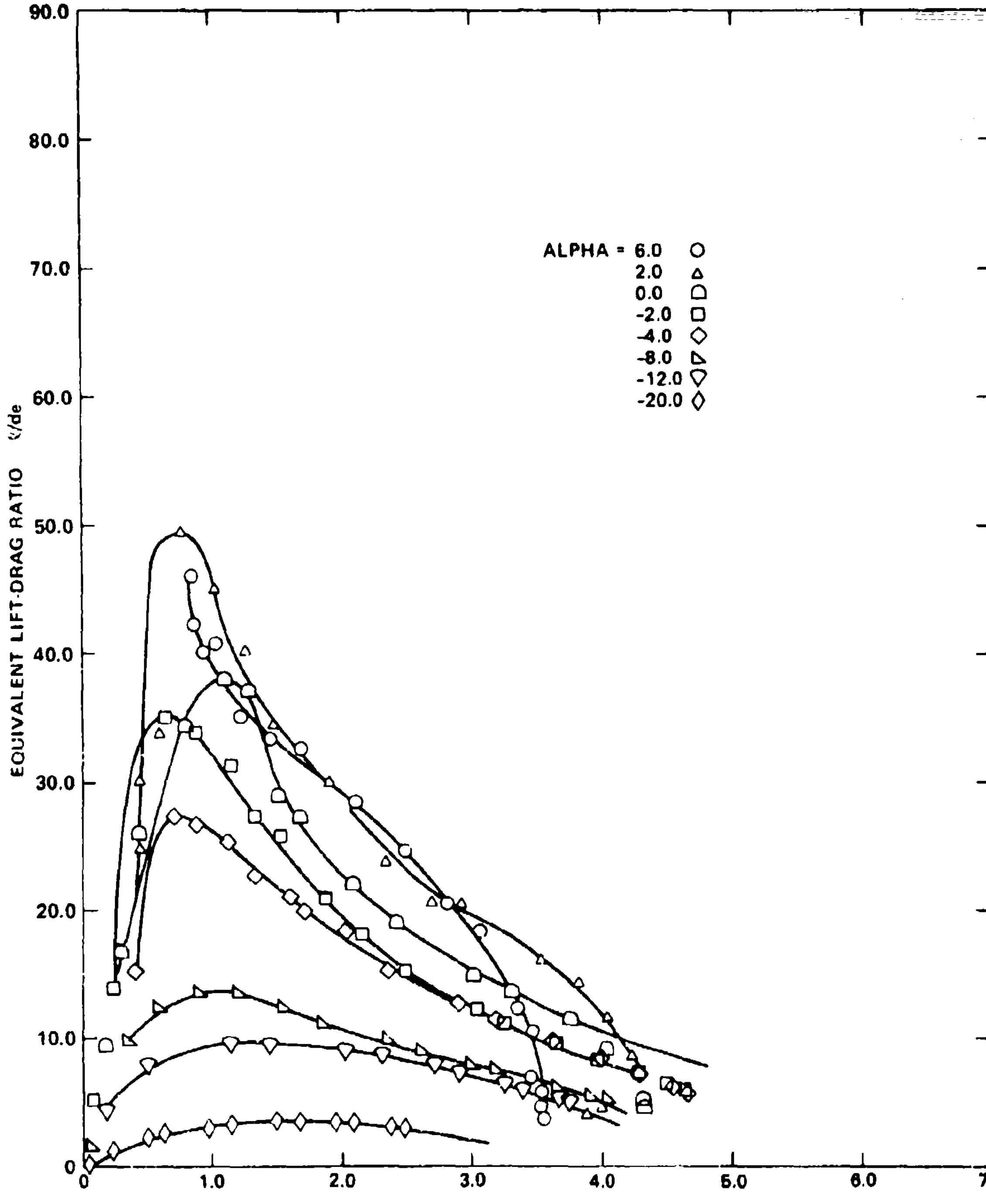

Figure 21 - Model NCCR 1510-7067N Equivalent Lift-to-Drag Ratio, h/c = 0.0015

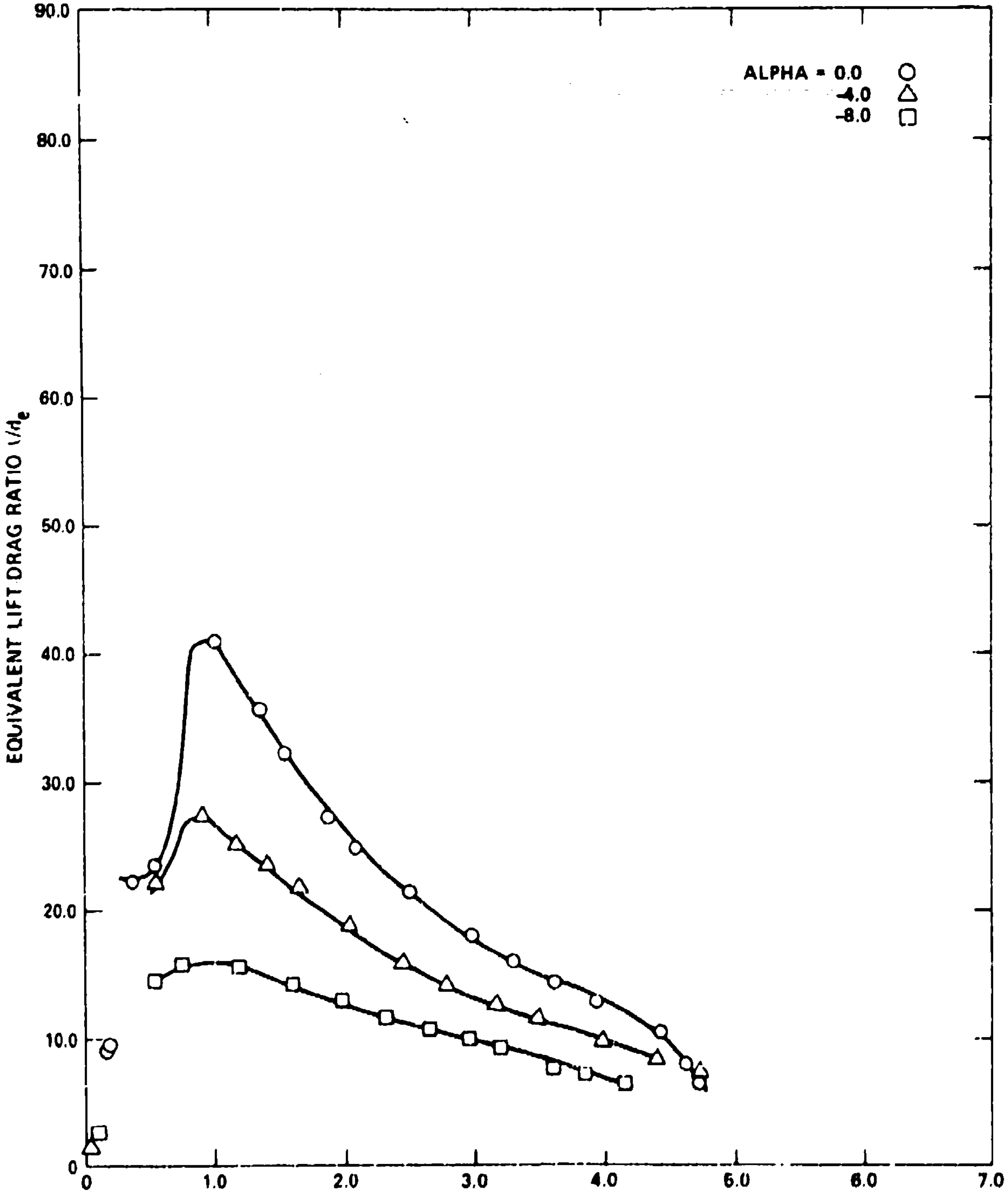

Figure 22 - Model NCCR 1510-7067N Equivalent Lift-to-Drag Ratio, h/c = 0.0022

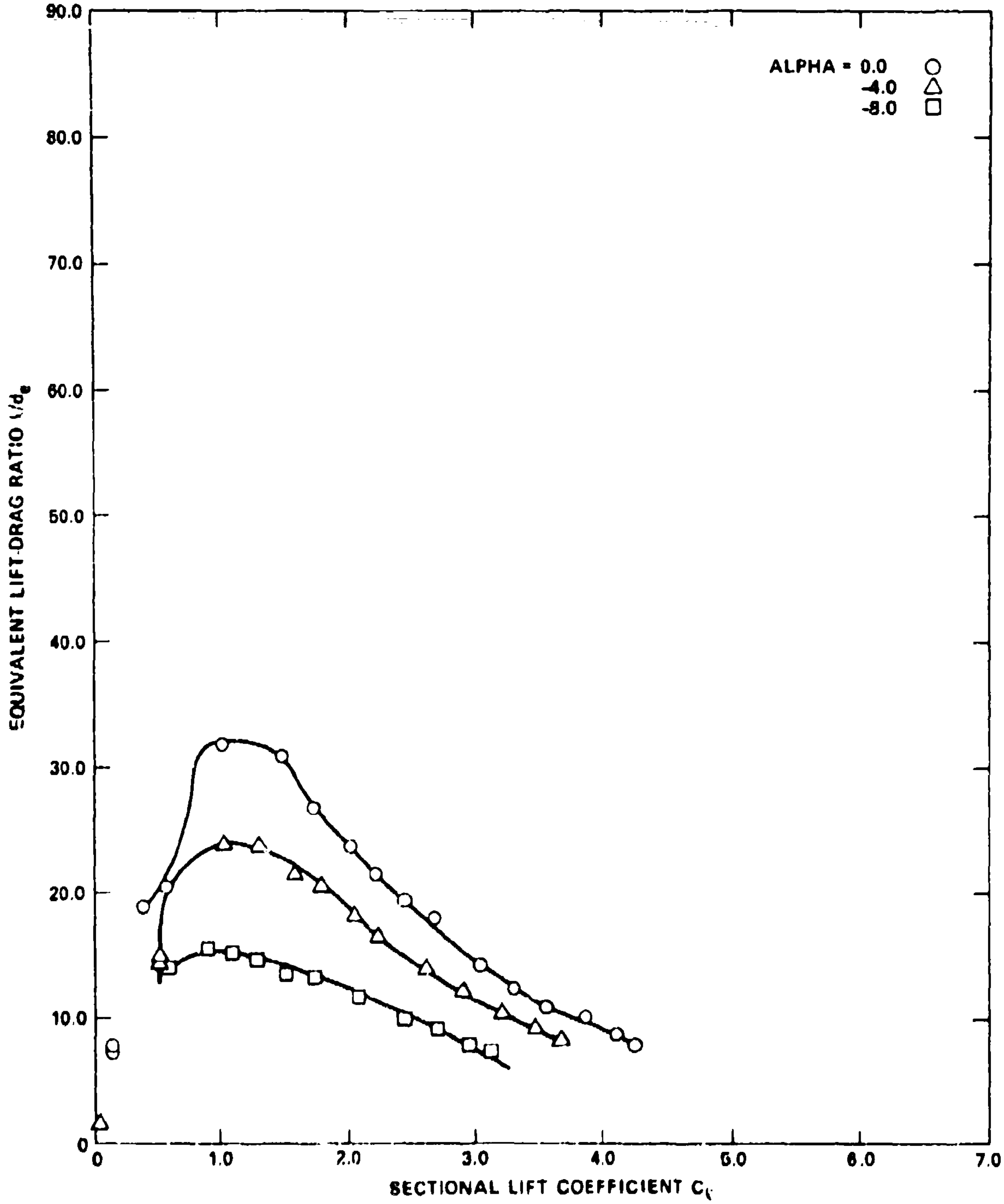

Figure 23 - Model NCCR 1510-7067N Equivalent Lift-to-Drag Ratio, h/c = 0.003

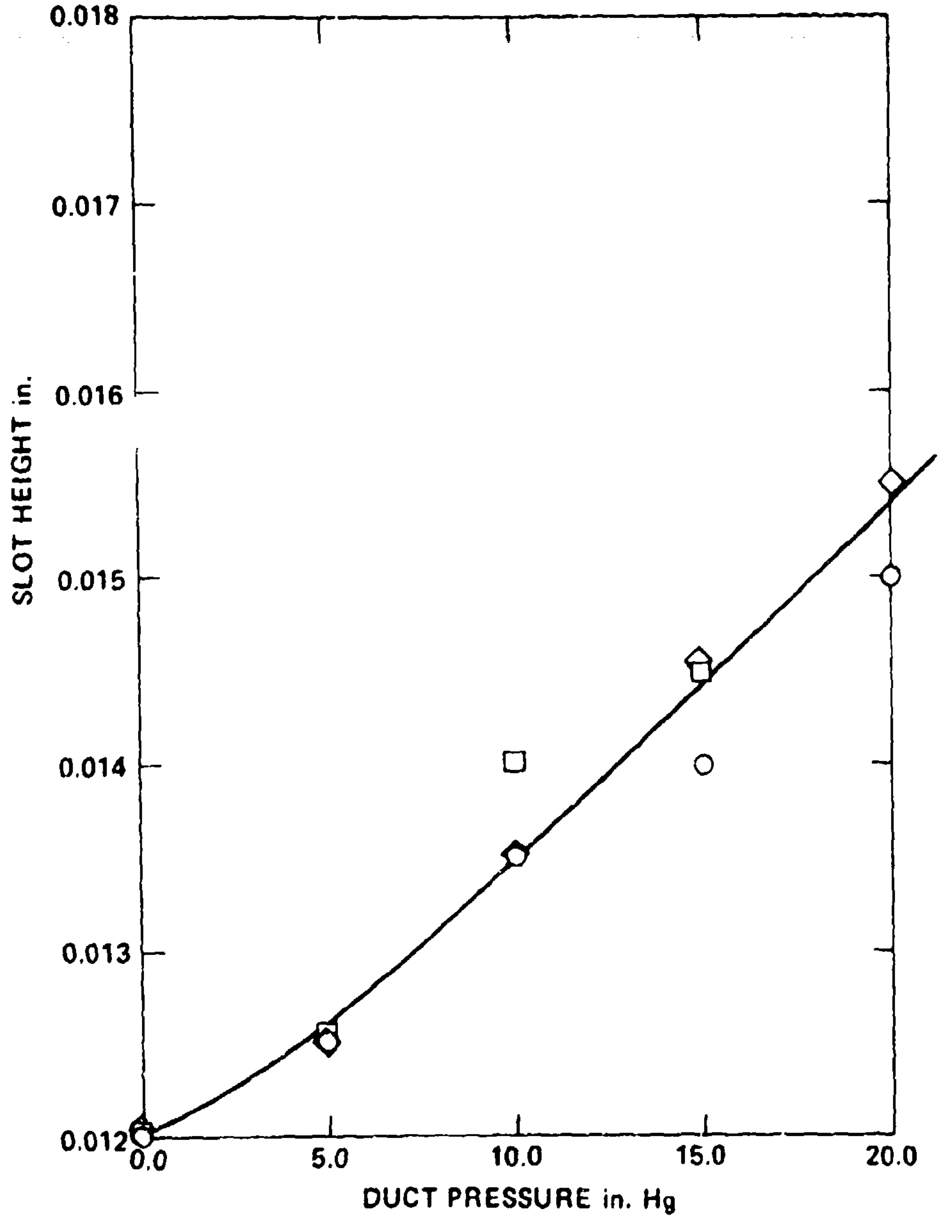

Figure 24 - Model NCCR 1510-7567S Variation of Slot Height with Duct Pressure

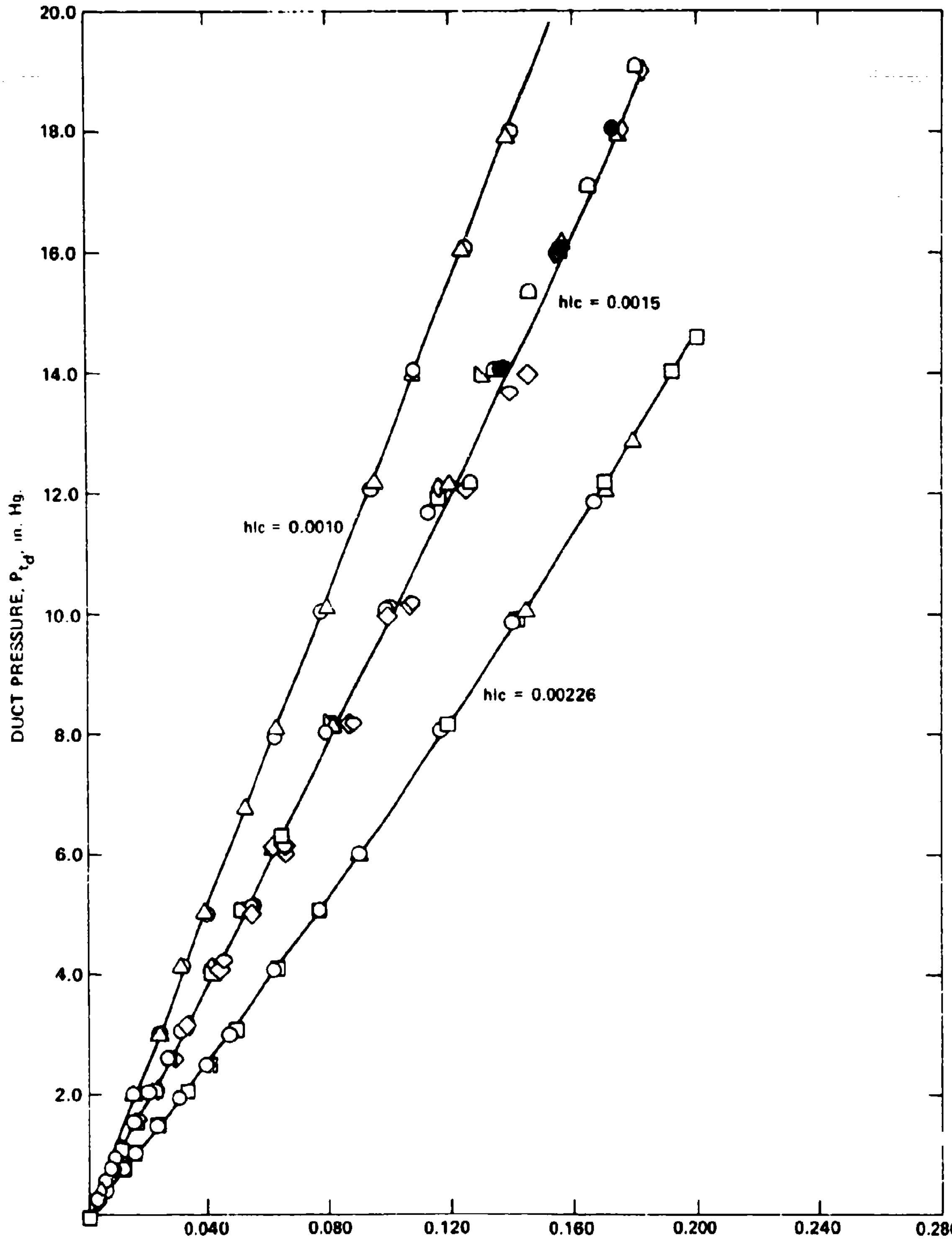

Figure 25 - Variation of Momentum Coefficient with Duct Pressure and Slot Height

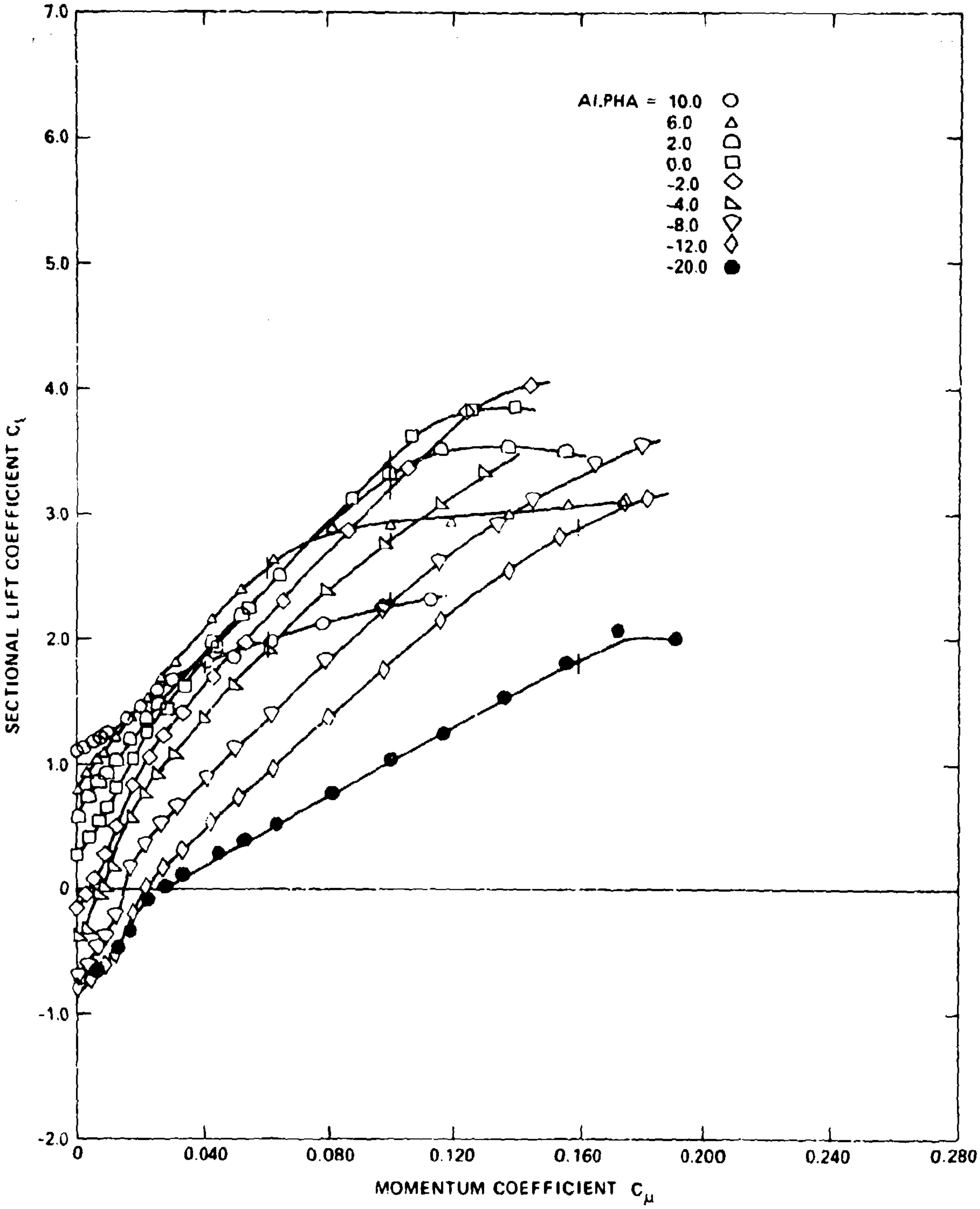

Figure 26 - Model NCCR 1510-7567S Lift Variation with Momentum Coefficient, h/c = 0.0015

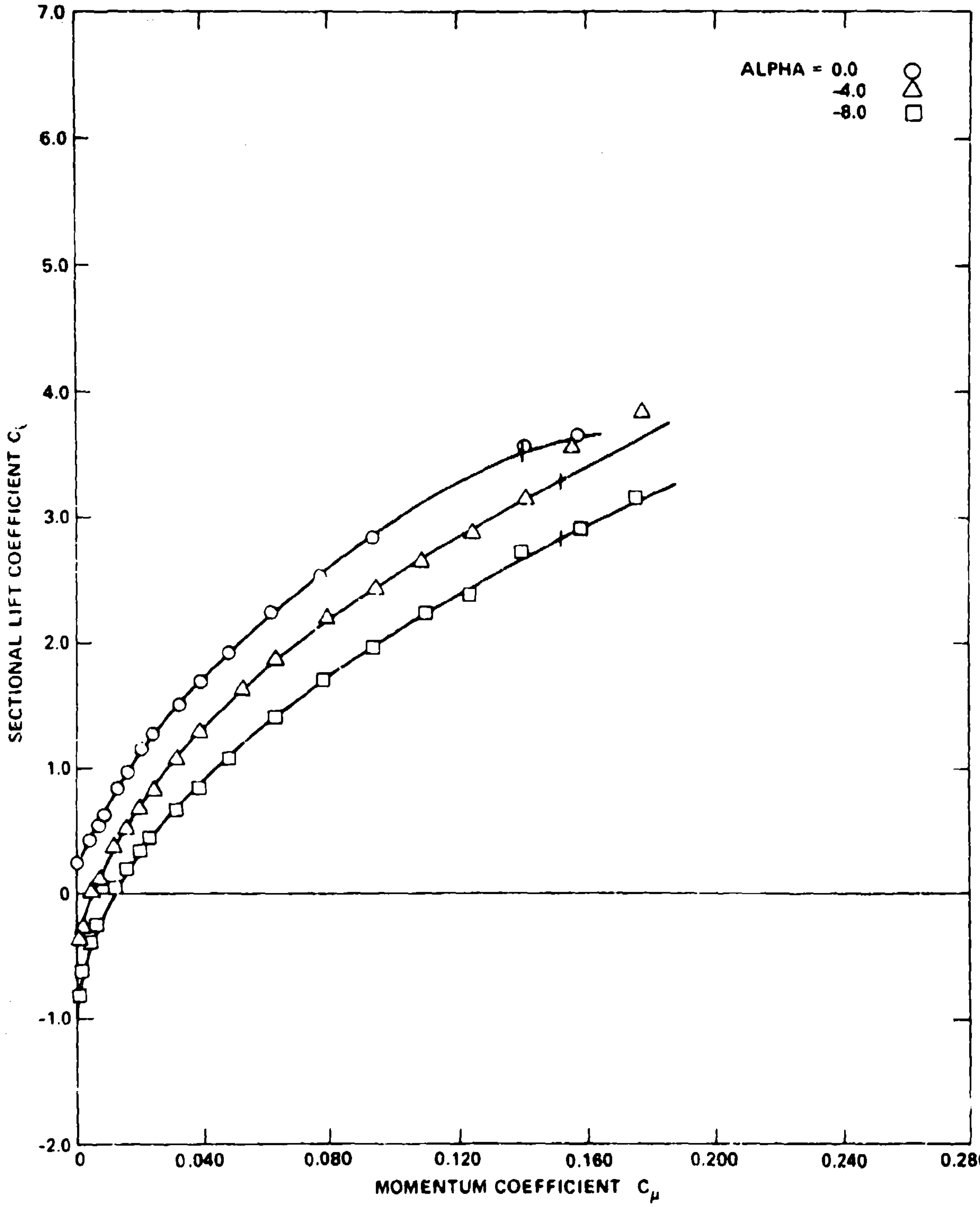

Figure 27 - Model NCCR 1510-7567S Lift Variation with Momentum Coefficient, h/c = 0.001

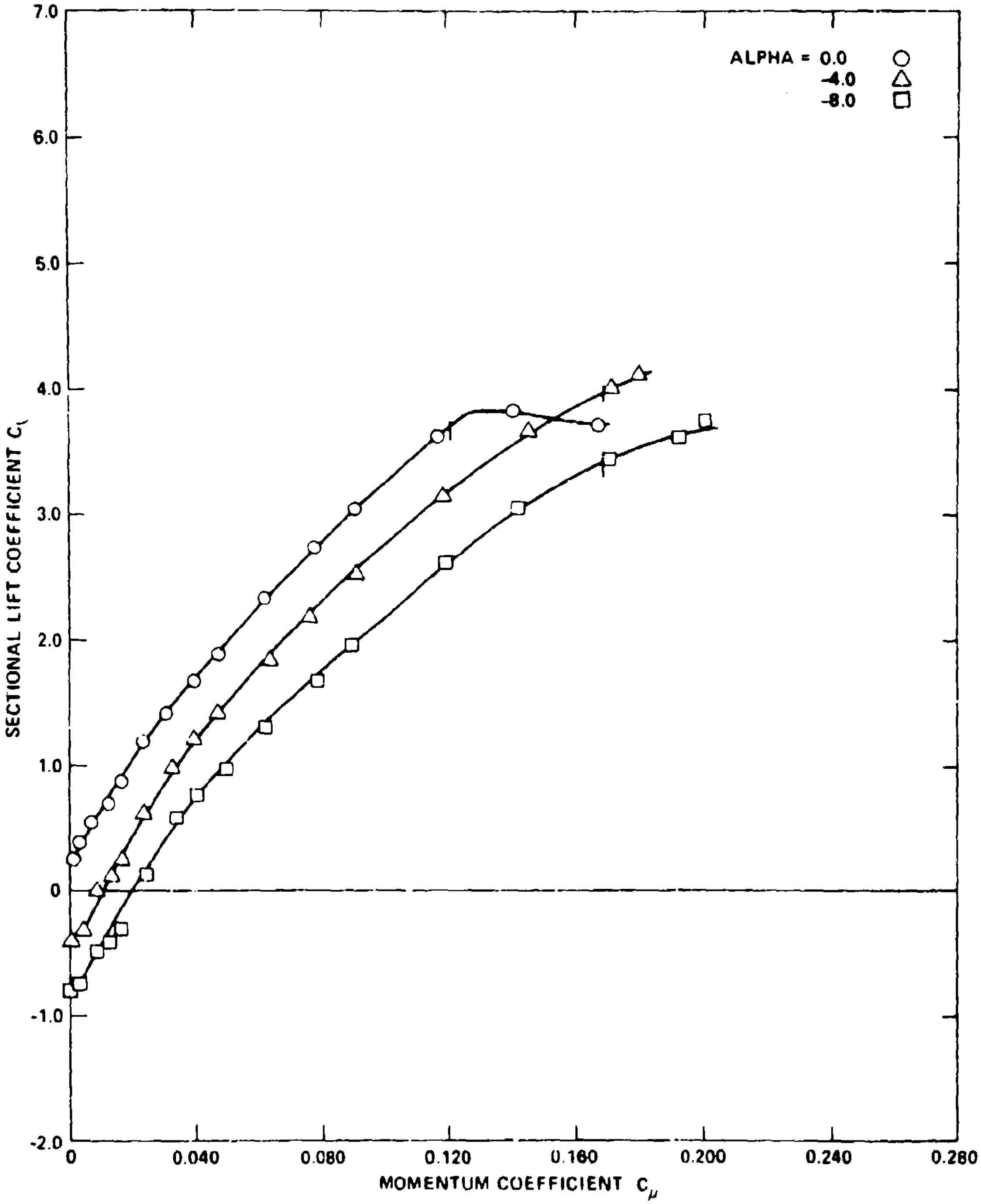

Figure 28 - Model NCCR 1510-7567S Lift Variation with Momentum Coefficient, h/c = 0.00226

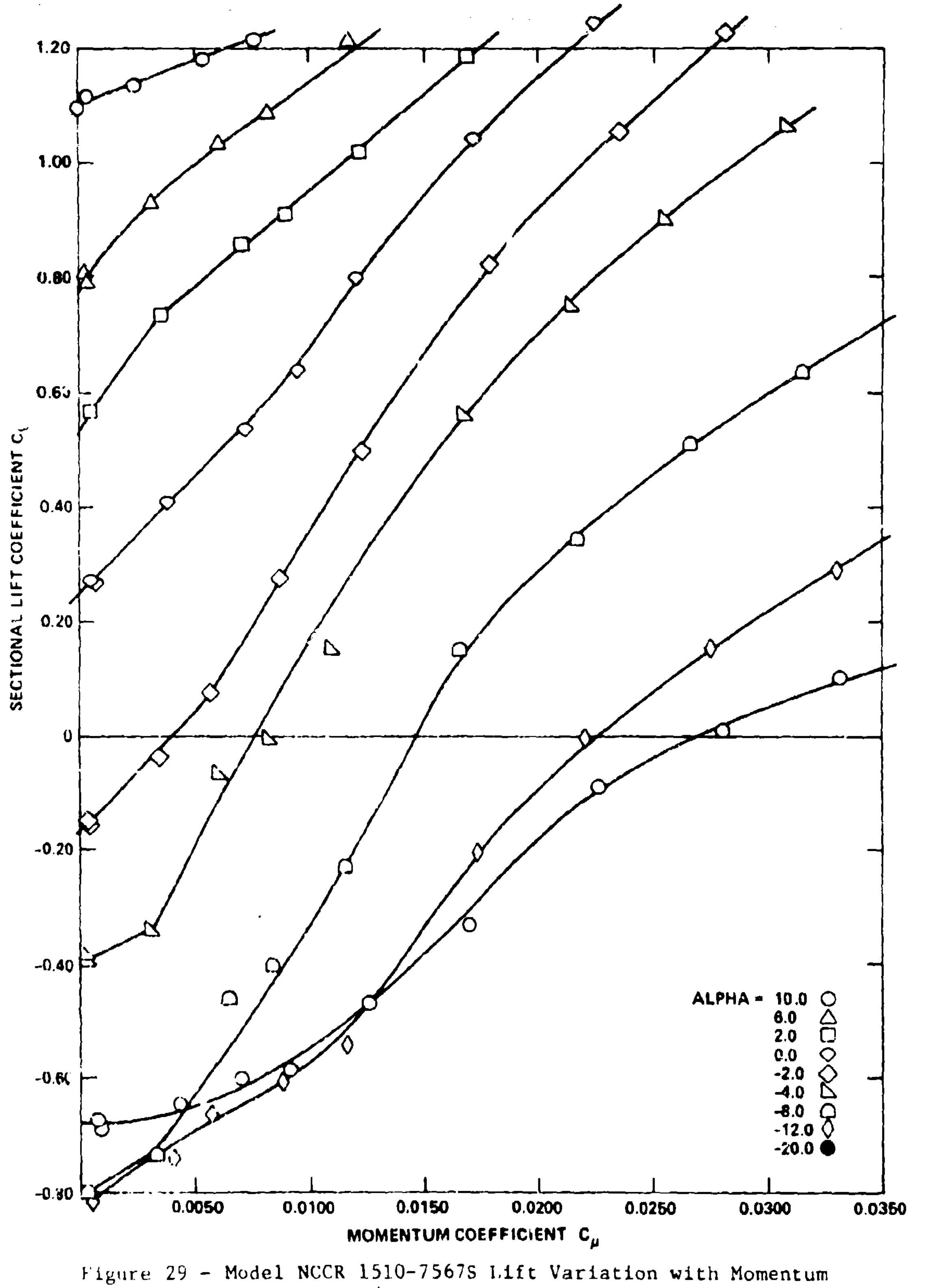

Figure 29 - Model NCCR 1510-7567S Lift Variation with Momentum Coefficient, h/c = 0.0015 (Expanded Scale)

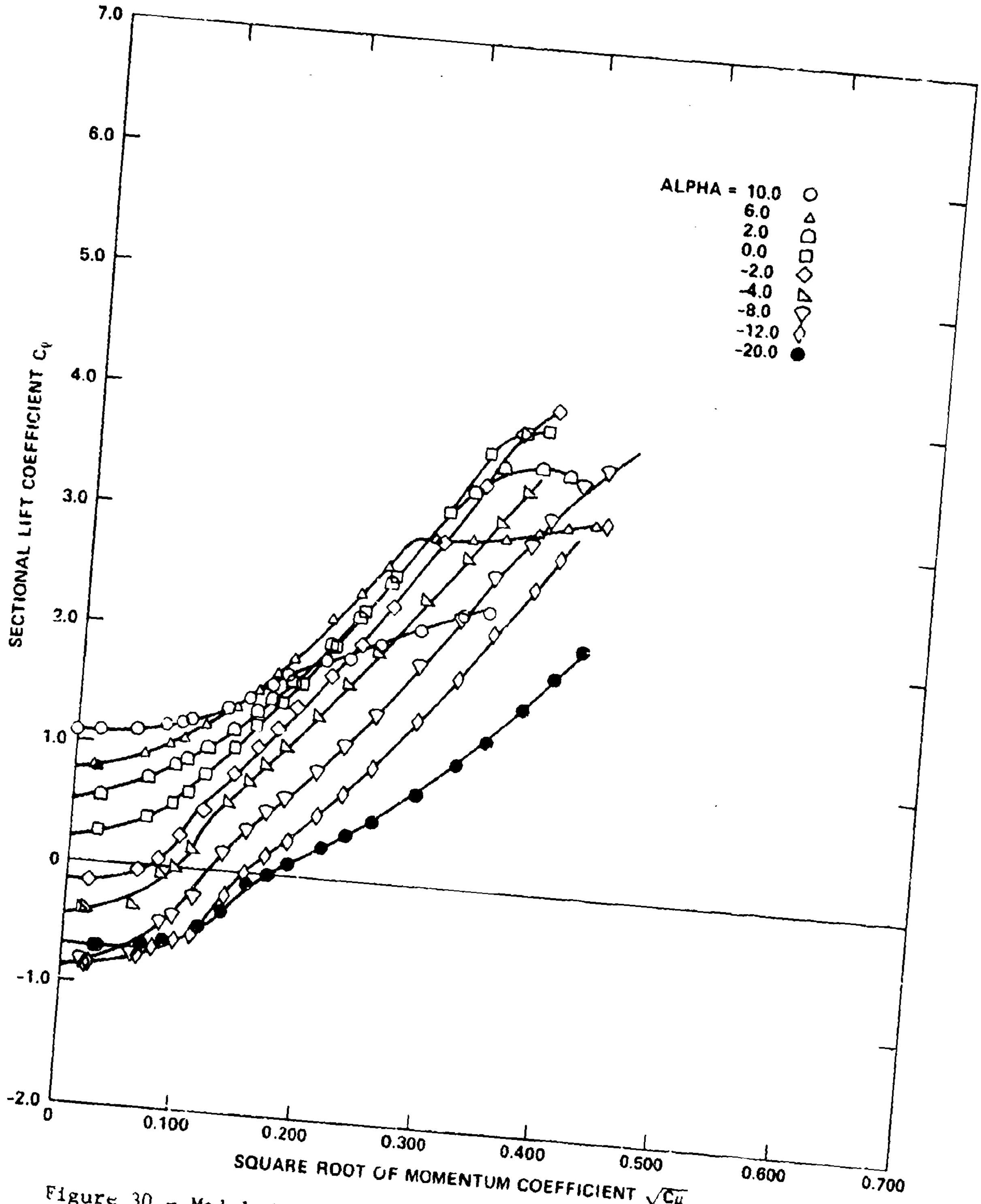

Figure 30 - Model NCCR 1510-7567S Lift Variation with the Square Root of Momentum Coefficient, h/c = 0.0015

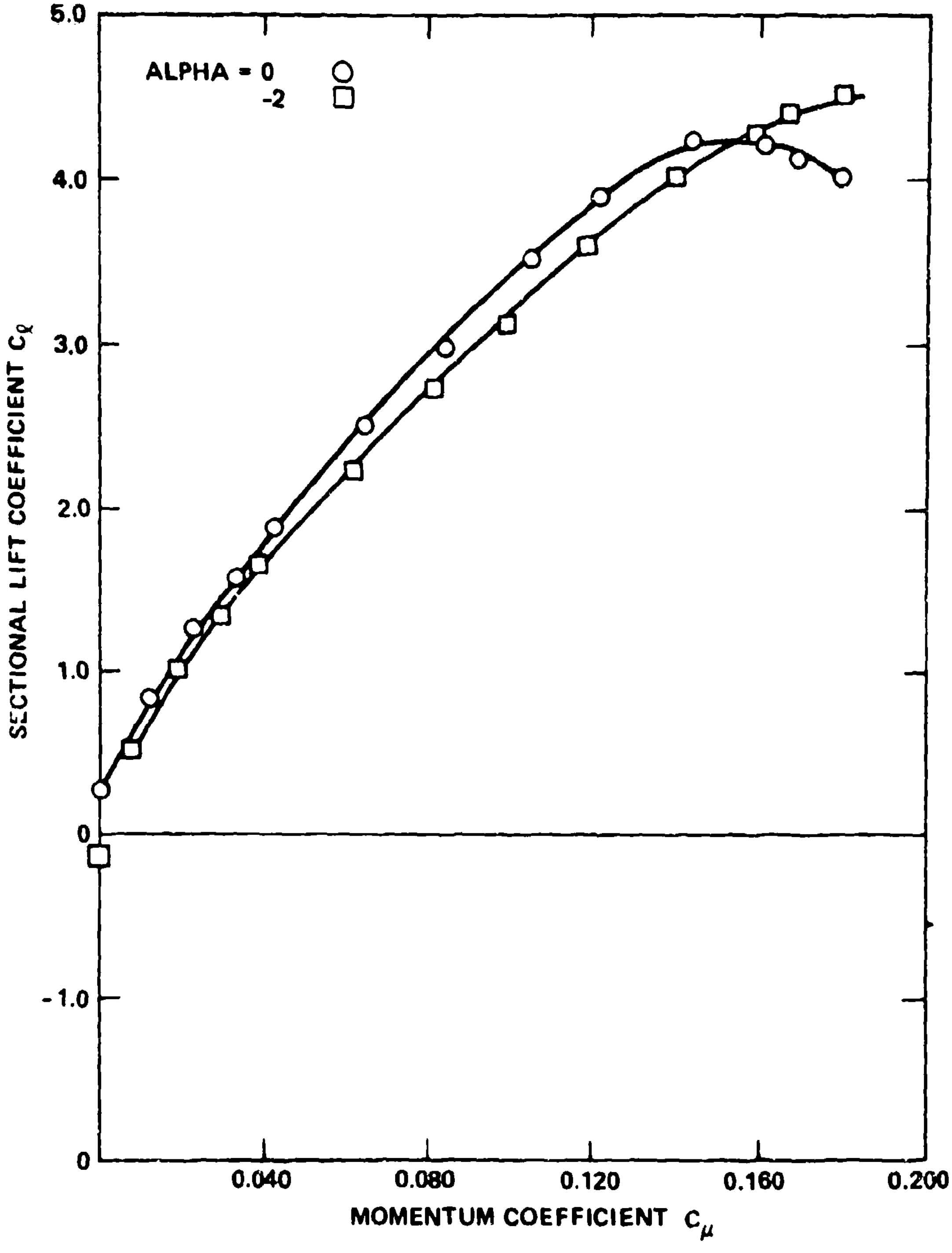

Figure 31 - Model NCCR 1510-7567S Lift Variation with Momentum Coefficient, h/c = 0.0015 (Model Raised)

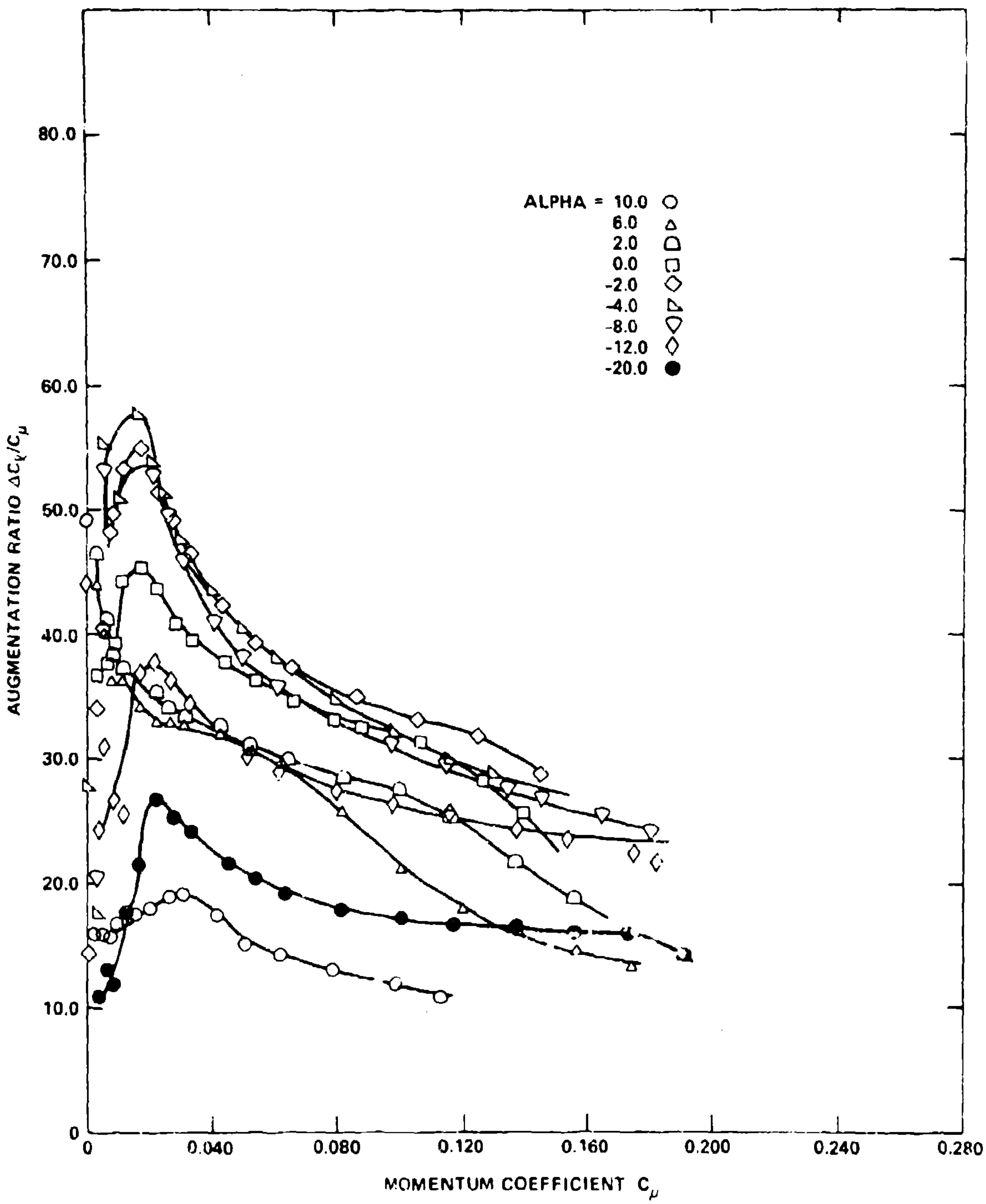

Figure 32 - Model NCCR 1510-7567S Lift Augmentation, h/c = 0.0015

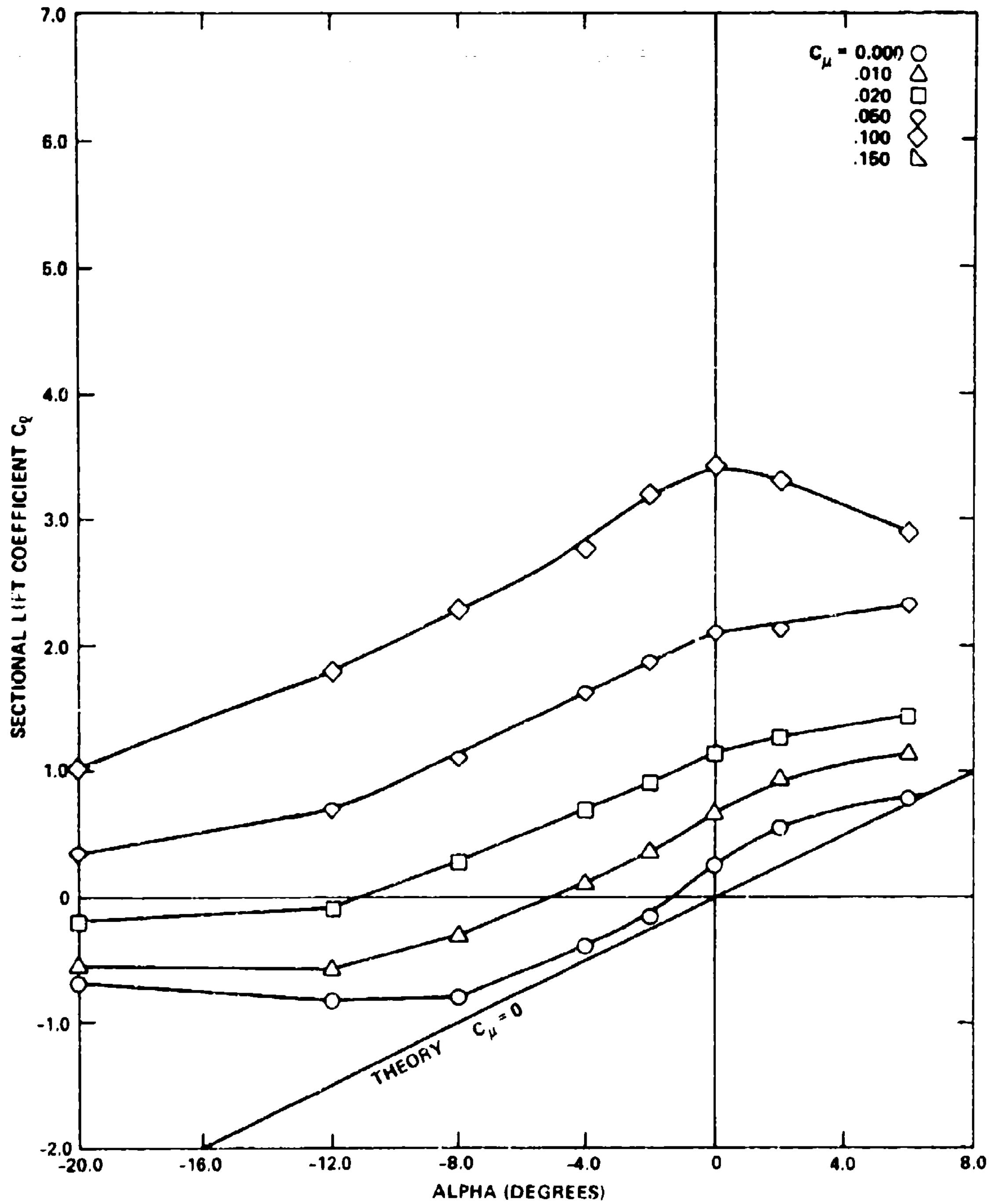

Figure 33 - Model NCCR 1510-7567S Lift Variation with Geometric Angle of Attack, h/c = 0.0015

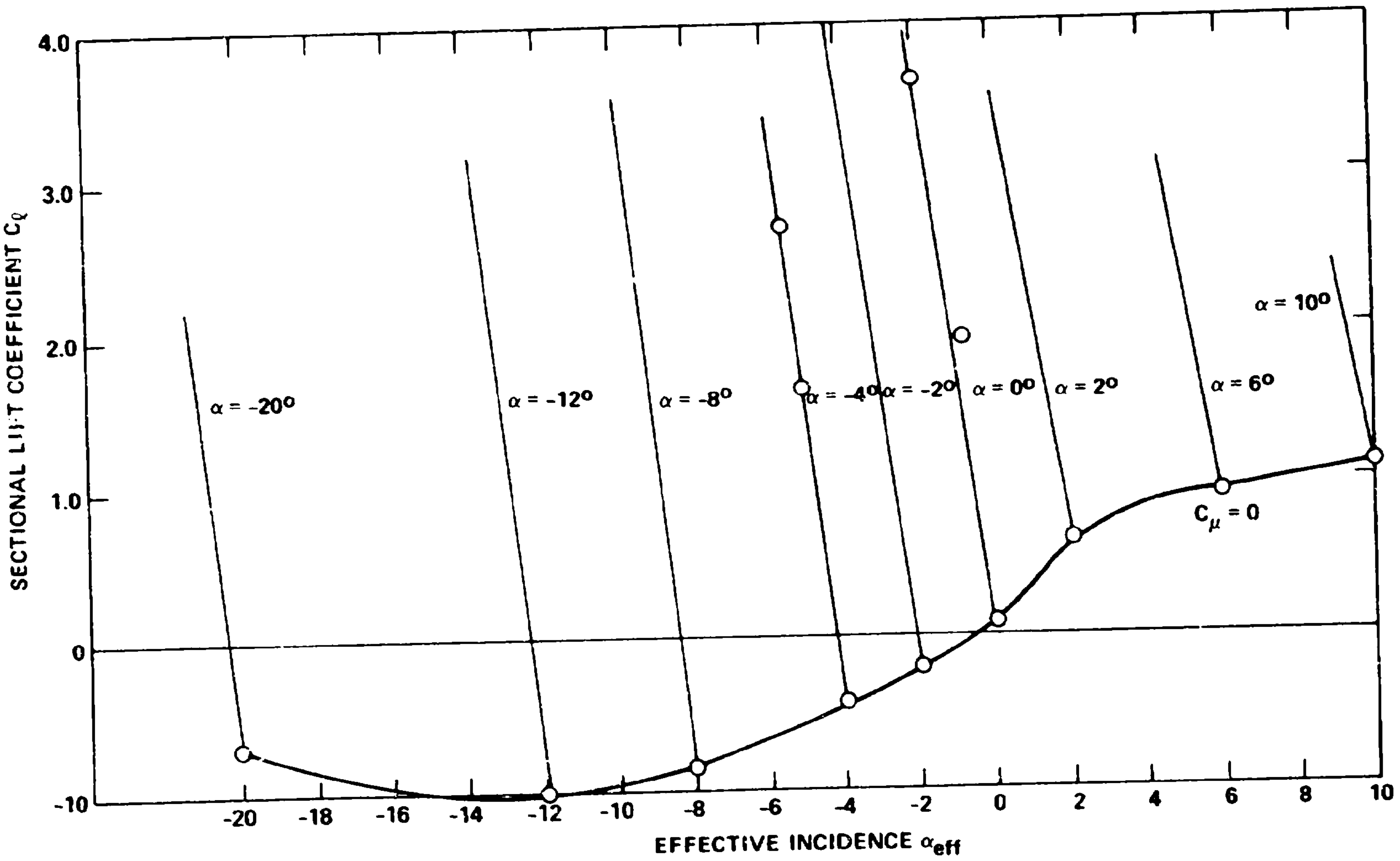

Figure 34 - Model NCCR 1510-7567S Induced Angle Corrections to Geometric Incidence

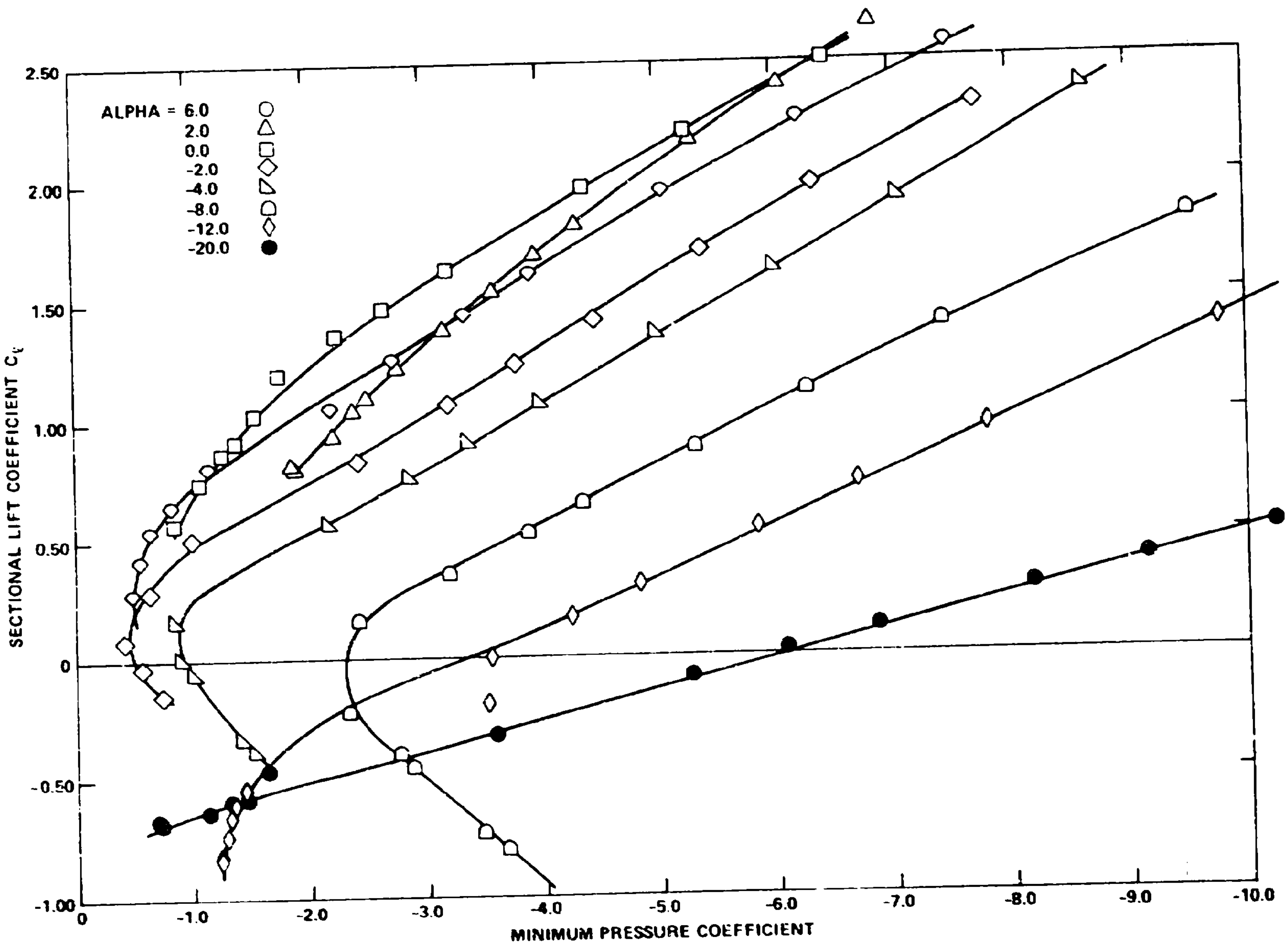

Figure 35 - Model NCCR 1510-7567S Minimum Pressure Coefficient, h/c = 0.0015

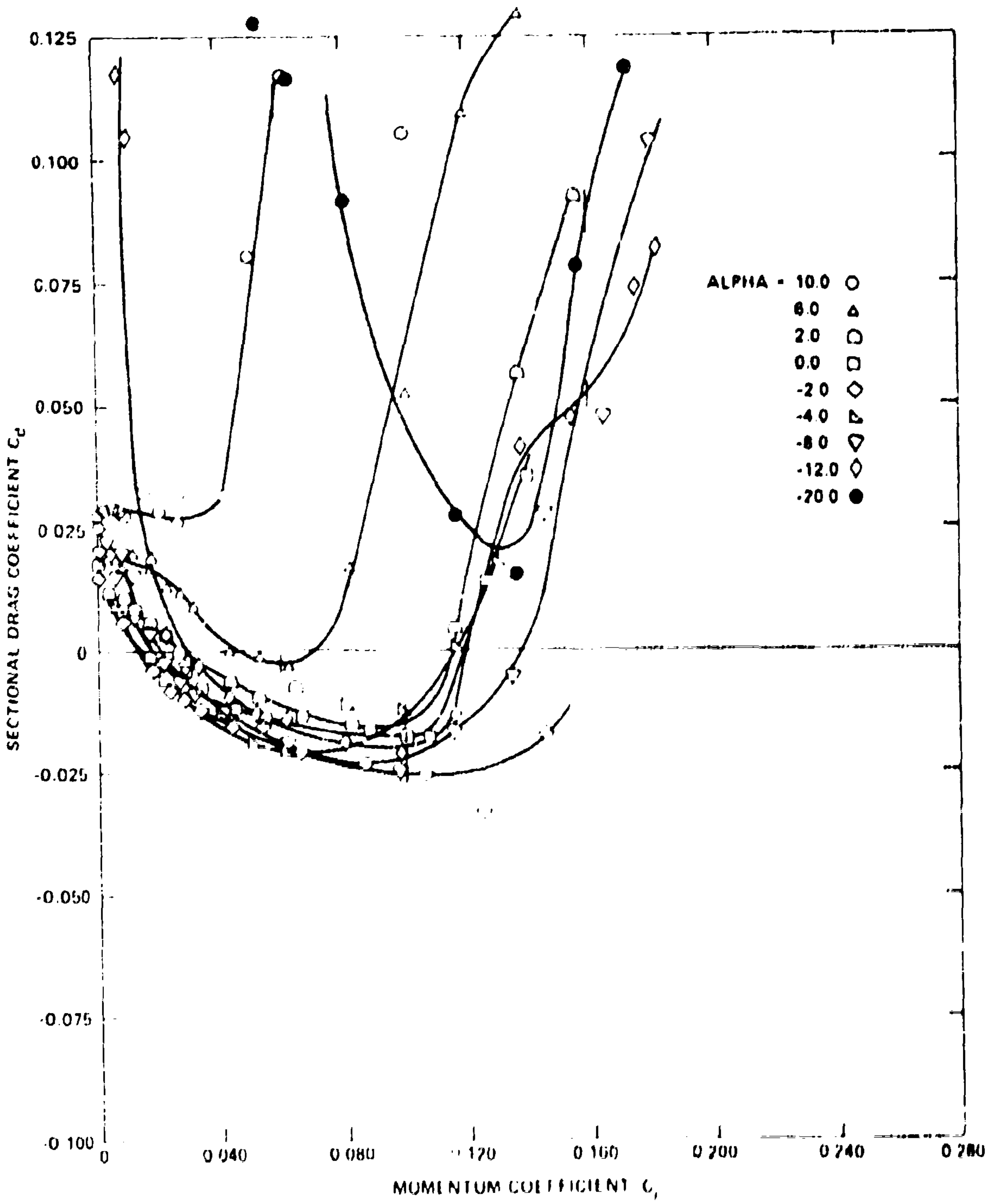

Figure 36 - Model NCCR 1510-7567S Drag Coefficient Variation with Momentum Coefficient, h/c = 0.0015

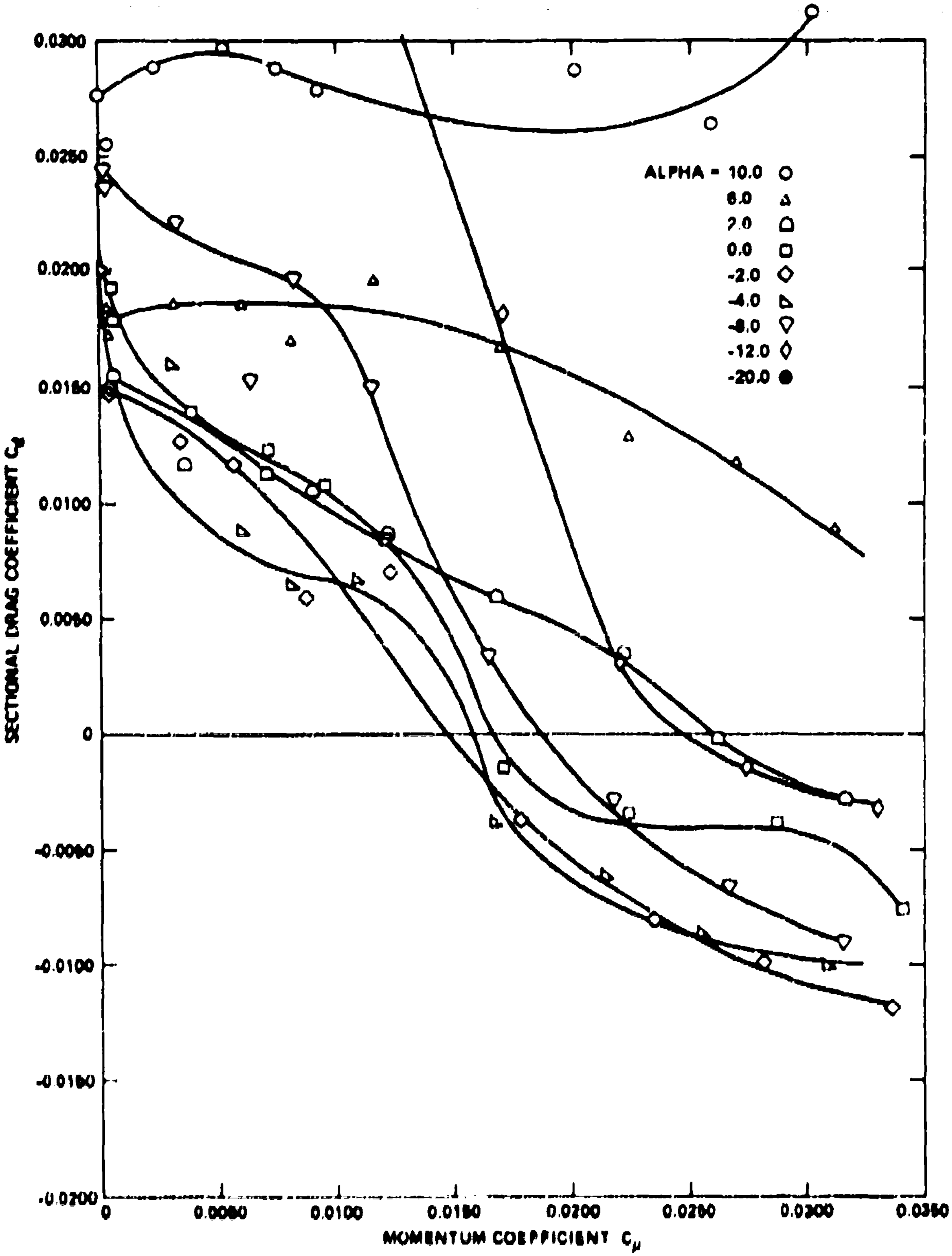

Figure 37 - Model NCCR 1510-7567B Drag Coefficient Variation with Momentum Coefficient, h/c = 0.0015 (Expanded Scale)

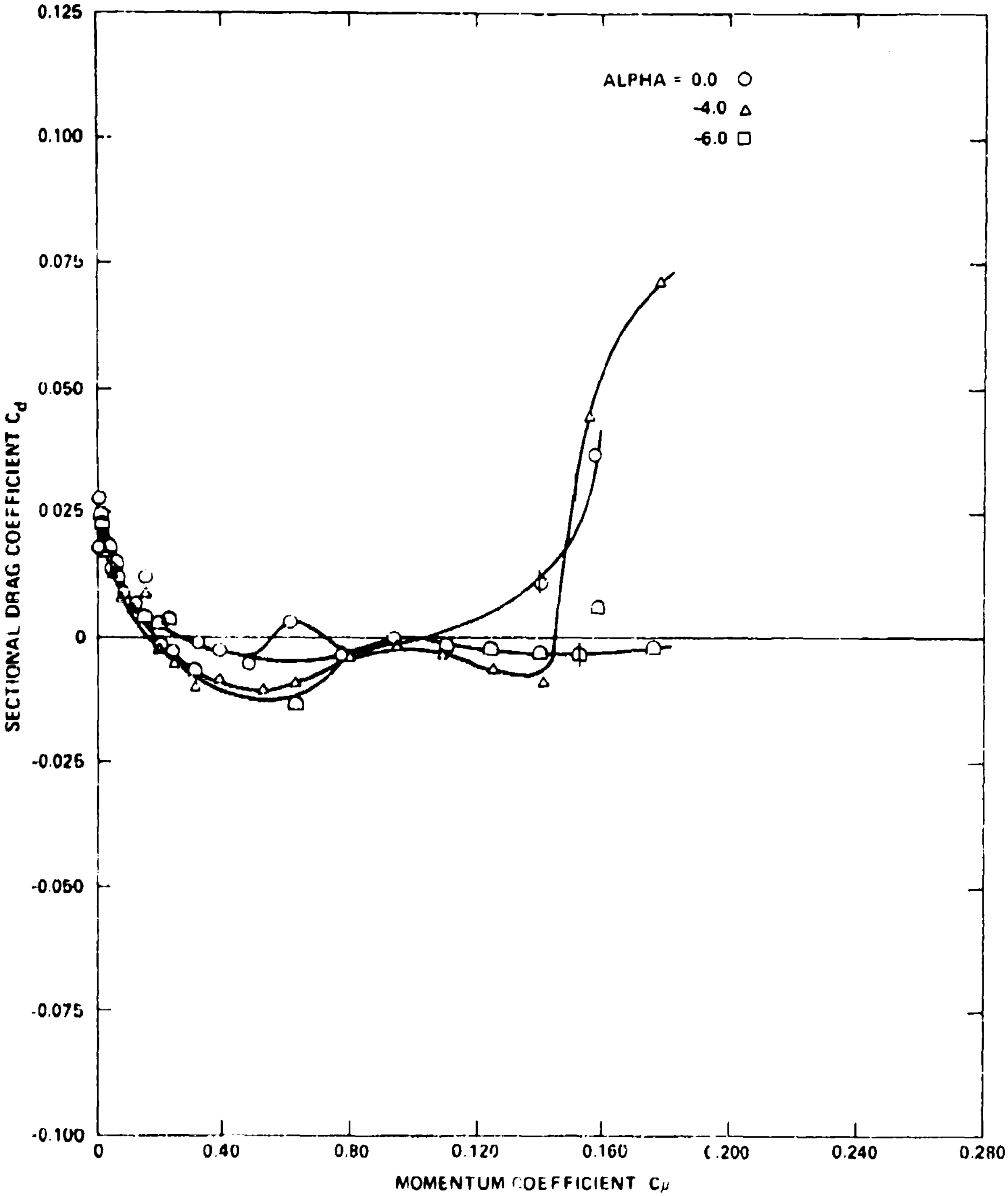

Figure 38 - Model NCCR 1510-7567S Drag Coefficient Variation with Momentum Coefficient, h/c = 0.001

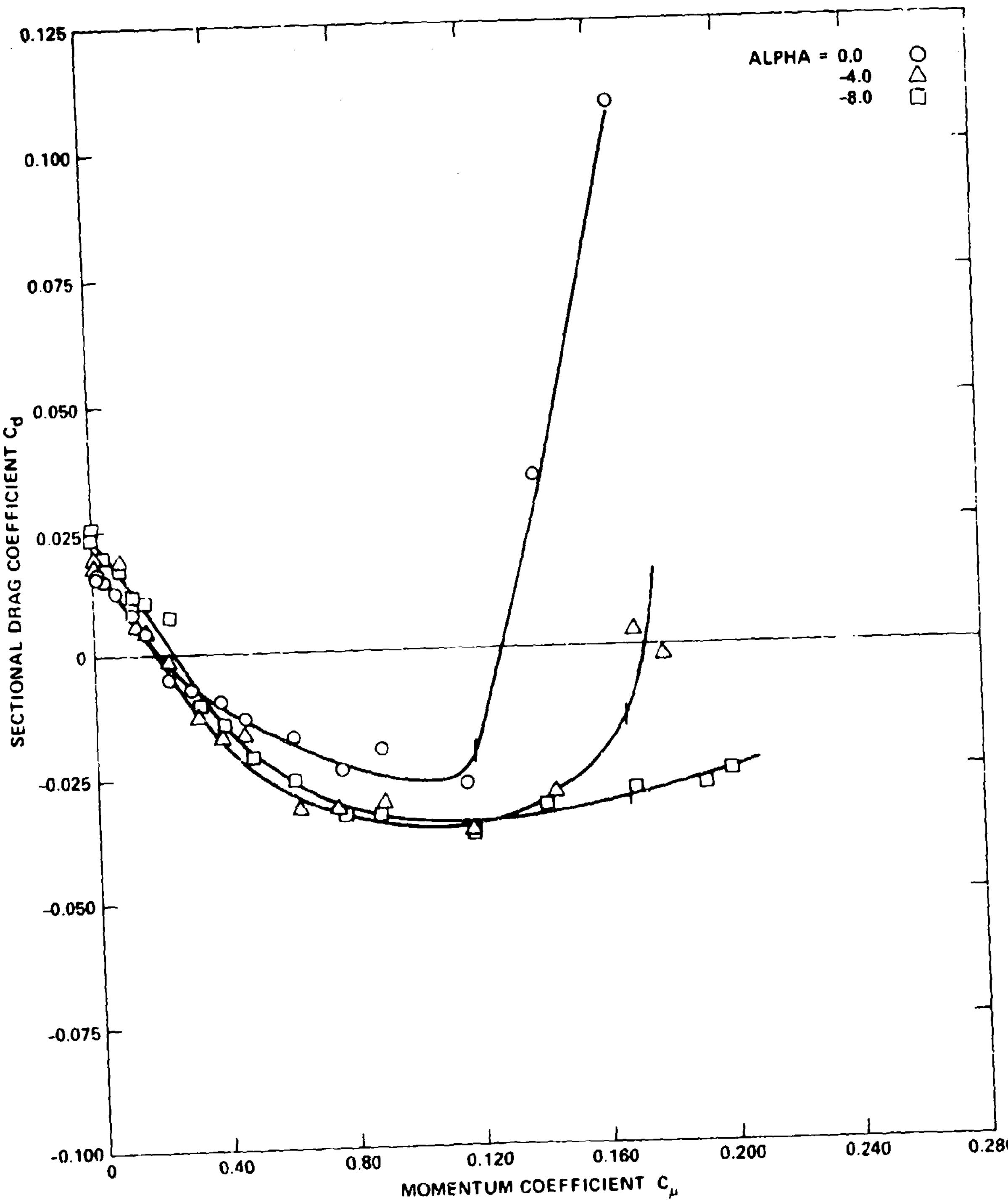

Figure 39 - Model NCCR 1510-7567S Drag Coefficient Variation with Momentum Coefficient, h/c = 0.00226

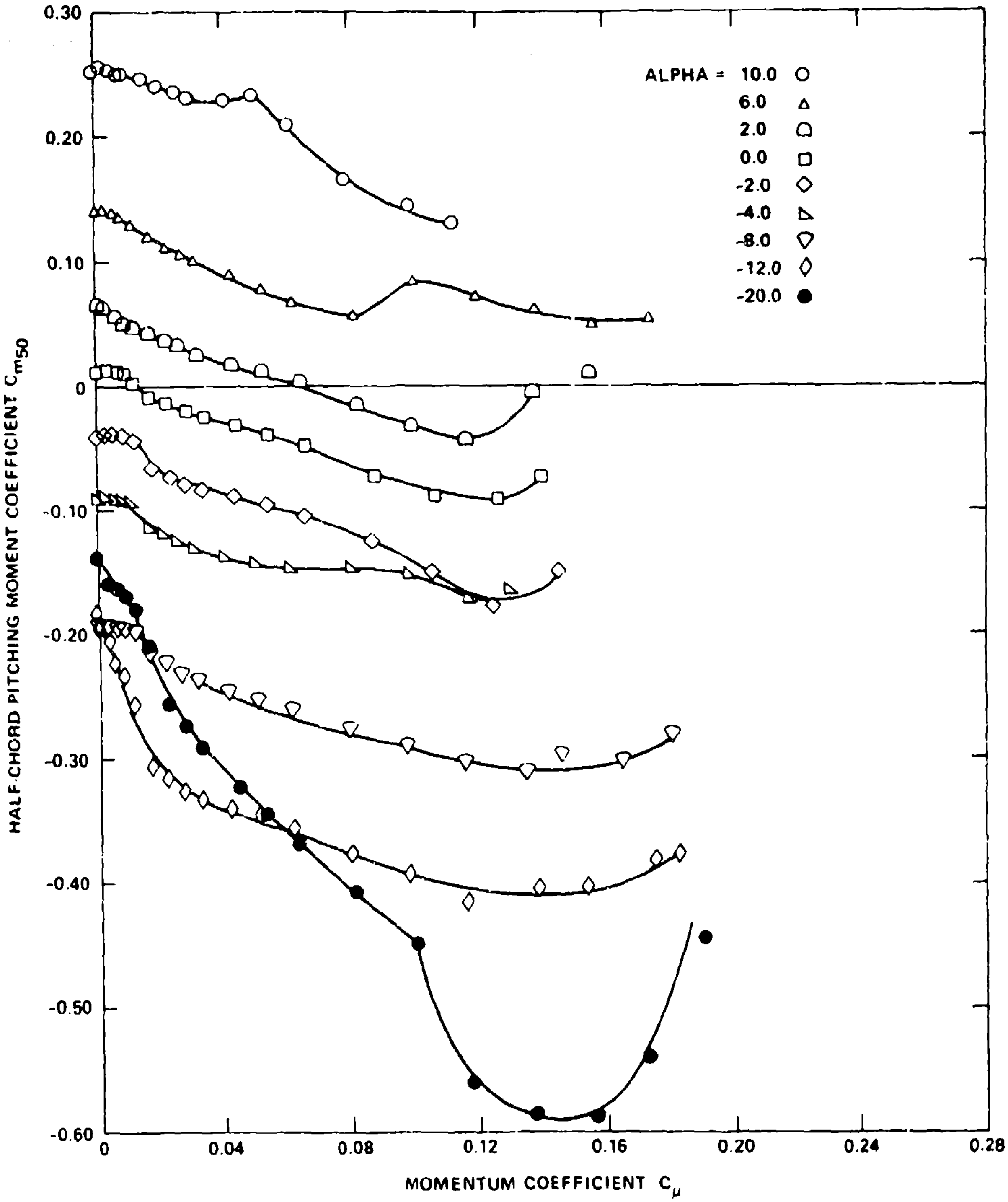

Figure 40 - Model NCCR 1510-7567S Variation in Half-Chord Pitching Moment Coefficient, h/c = 0.0015

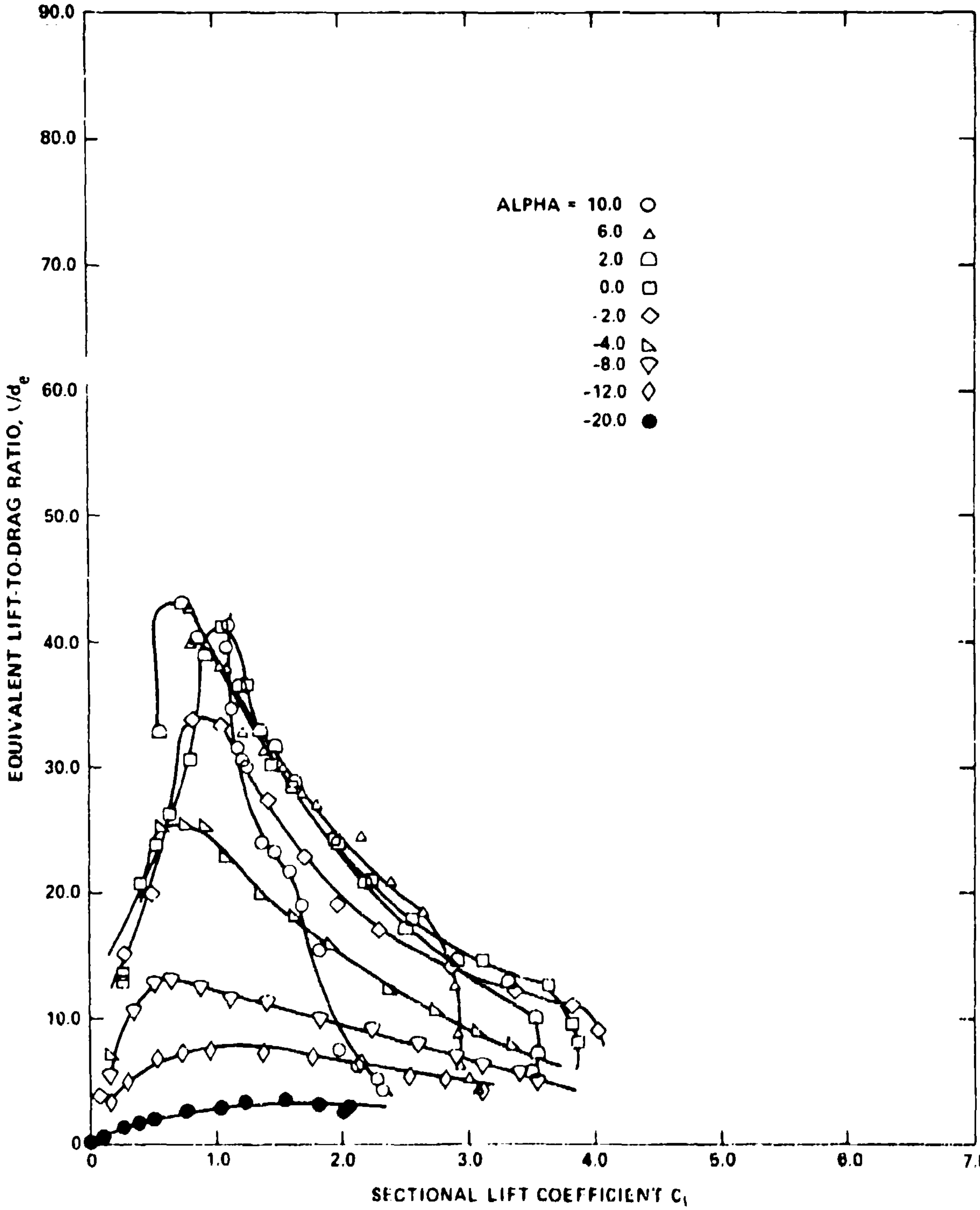

Figure 41 - Model NCCR 1510-7567S Equivalent Lift-to-Drag Ratio, h/c = 0.0015

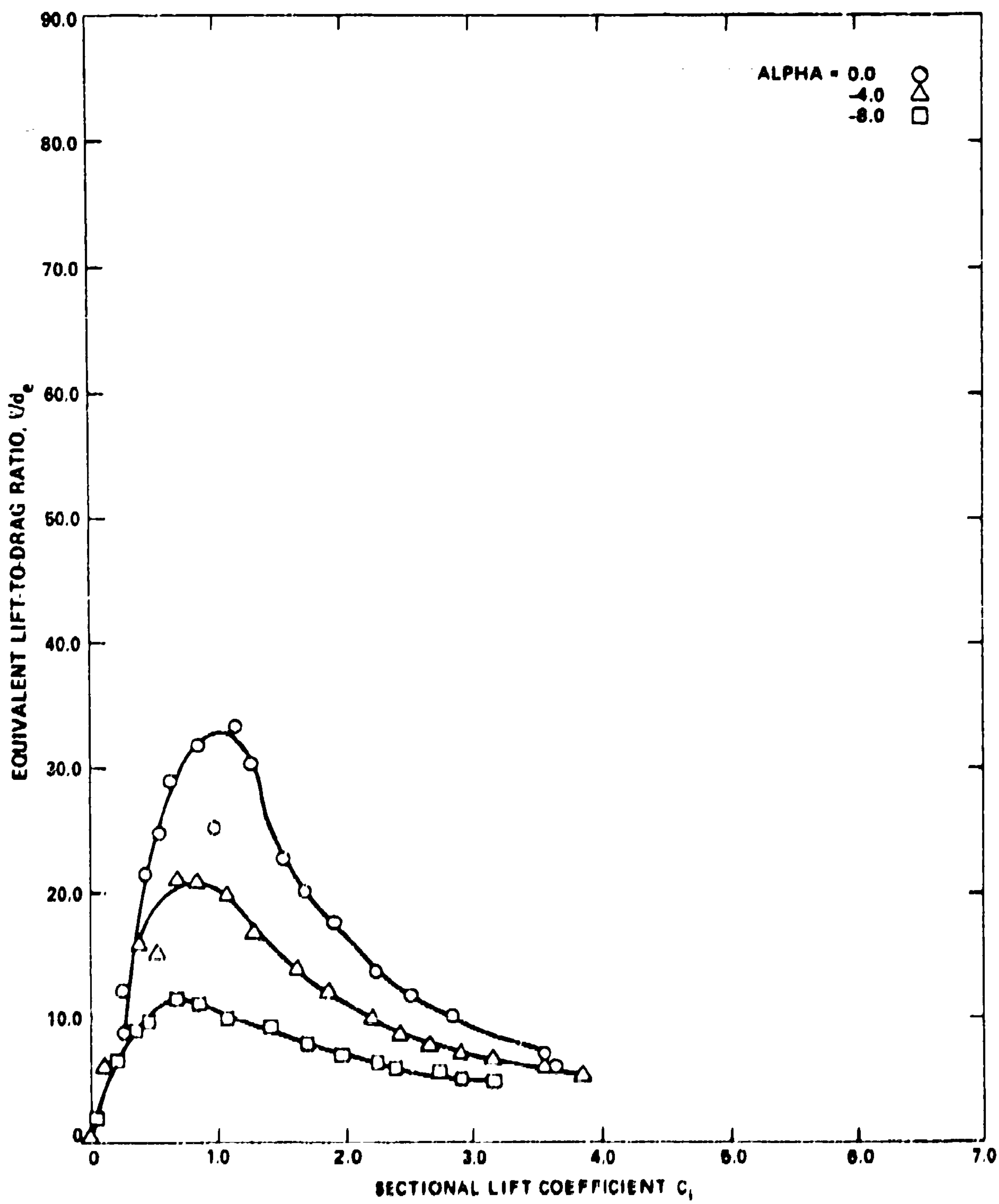

Figure 42 - Model NCCR 1510-7567B Equivalent Lift-to-Drag Ratio, h/c = 0.001

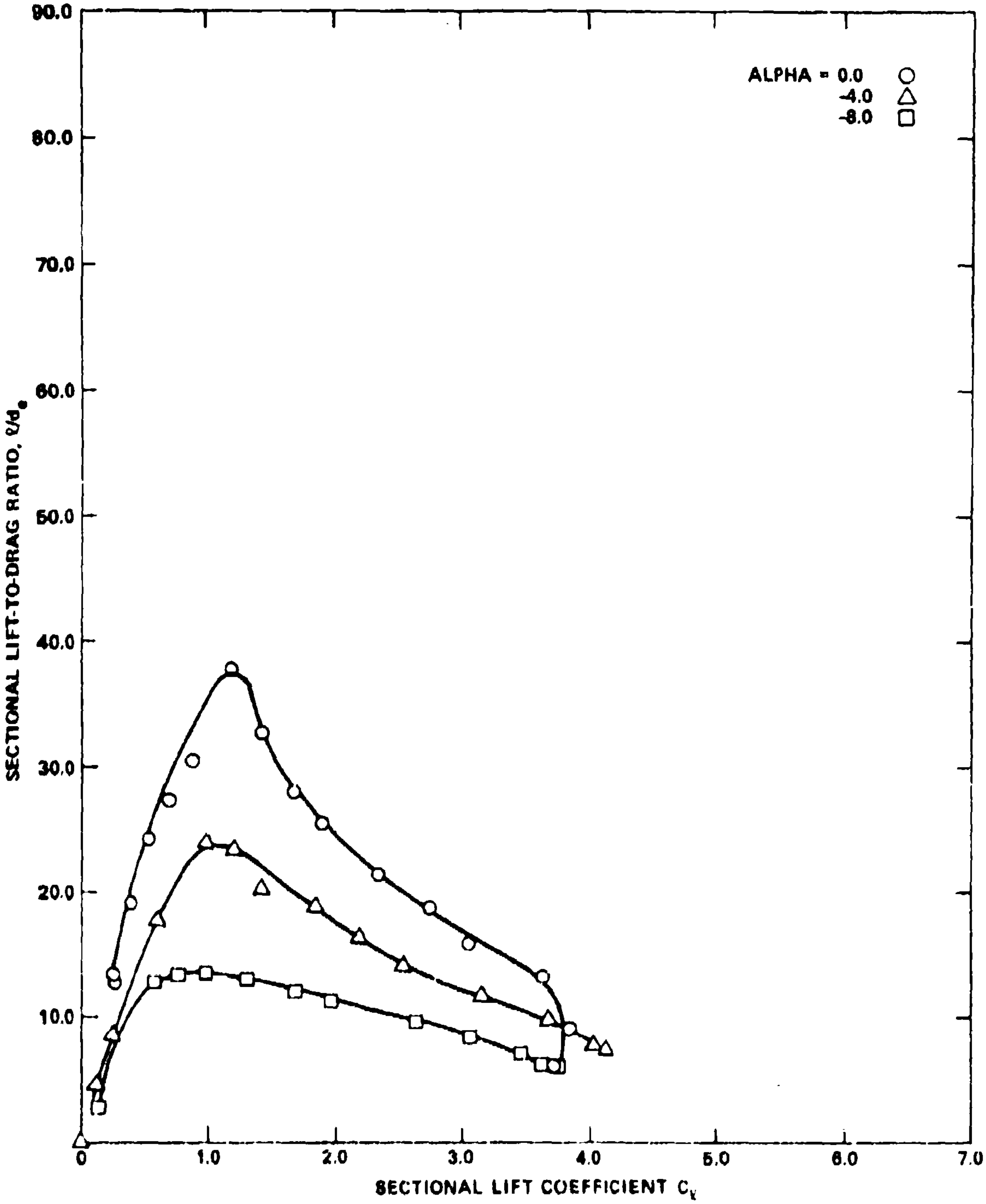

Figure 43 - Model NCCR 1510-7567S Equivalent Lift-to-Drag Ratio, h/c = 0.00226

TABLE 1 — DESIGNATION FOR CCR AIRFOILS

NCCR 1516-7464N

Navy Circulation Control Rotor (NCCR)

Descriptor for Coanda Surface (N):

- E — elliptical
- C — circular arc
- N — nominal circular arc
- S — spiral
- D — dual blowing (double ended)

Trailing Edge Bluffness (64):

Airfoil thickness ratio in percent actual chord measured at slot location (6.4-percent thickness as shown)

Slot Location (74):

This is the second and third digit of the slot location measured from the nose in percent actual chord (97.4 percent as shown)

Camber (16):

The maximum camber in percent virtual chord is one-tenth of this value (1.6 percent as shown)

Thickness (15):

Airfoil thickness ratio in percent virtual chord (15 percent as shown)

TABLE 2 – TWO-DIMENSIONAL MODEL COORDINATES FOR UPPER AND LOWER SURFACES –MODEL NCCR 1510-7067N

Upper Surface X	Upper Surface Y		Lower Surface X	Lower Surface Y	
00.0000	00.0000	LEADING EDGE	00.0000	-00.0000	LEADING EDGE
00.0100	00.0731		00.0100	-00.0514	
00.0300	00.1067		00.0300	-00.0763	
00.0500	00.1330		00.0500	-00.1008	
00.0800	00.1596		00.0800	-00.1270	
00.1000	00.1737		00.1000	-00.1415	
00.1200	00.1857		00.1200	-00.1518	
00.1500	00.2034		00.1500	-00.1685	
00.1800	00.2202		00.1800	-00.1810	
00.2100	00.2363		00.2100	-00.1917	
00.2400	00.2507		00.2400	-00.2021	
00.4000	00.3164		00.4000	-00.2479	
01.0000	00.4715		01.0000	-00.3538	
01.6000	00.5719		01.6000	-00.4251	
02.2000	00.6310		02.2000	-00.4841	
02.8000	00.6621		02.8000	-00.5125	
03.4000	00.6847		03.4000	-00.5270	
04.0000	00.6971		04.0000	-00.5267	
04.6000	00.6894		04.6000	-00.5150	
05.2000	00.6586		05.2000	-00.5019	
05.6000	00.6354		05.6000	-00.4878	
06.2000	00.5889		05.9700	-00.4719	
06.8000	00.5140		06.0542	-00.4618	
07.4000	00.3981		06.2000	-00.4512	
07.6000	00.3469		06.8000	-00.4054	
07.7500	00.2914		07.4000	-00.3397	
07.7800	00.2582		07.6500	-00.2972	
07.8000	00.2562		07.7500	-00.2731	
07.8300	00.2451		07.8000	-00.2549	
07.8600	00.2310		07.8300	-00.2459	
07.8800	00.2216		07.8600	-00.2298	
07.9000	00.2084		07.8800	-00.2144	
07.9200	00.1927		07.9000	-00.2069	
07.9400	00.1732		07.9200	-00.1933	
07.9600	00.1506		07.9400	-00.1728	
07.9800	00.1221		07.9600	-00.1528	
08.0000	00.0814		07.9800	-00.1200	
08.0100	00.0000	TRAILING EDGE	08.0000	-00.0791	
			08.0139	00.0000	TRAILING EDGE

TABLE 3

Two-Dimensional Model Coordinates for the Trailing Edge–Model NCCR 1510-7567S

Lower Surface X	Lower Surface Y	Upper Surface X	Upper Surface Y
5.5545	−0.501	7.2271	0.096
5.9167	−0.4838	7.2271	0.106
6.0789	−0.4591	7.34	0.123
6.6416	−0.4283	7.39	0.145
7.005	−0.3884	7.44	0.170
7.14	−0.3698	7.49	0.200
7.24	−0.3559	7.54	0.227
7.3692	−0.3354	7.59	0.249
7.442	−0.323	7.64	0.265
7.497	−0.3120	7.69	0.273
7.57	−0.2975	7.715	0.274
7.607	−0.29	7.74	0.273
7.643	−0.281	7.79	0.2650
7.69	−0.2670	7.81	0.258
7.74	−0.25	7.83	0.25
7.79	−0.225	7.85	0.2390
7.81	−0.211	7.87	0.2250
7.83	−0.198	7.89	0.2070
7.85	−0.18	7.91	0.183
7.87	−0.16	7.93	0.1510
7.89	−0.138	7.94	0.096
7.91	−0.107	7.955	0.04
7.93	−0.07		
7.95	−0.01		
7.955	−0.04		